3-21-2013

Cathodoluminescence and Thermoluminescence of Undoped LTB and LTB:A (A = Cu, Ag, Mn)

Zachary L. Hadfield

CATHODOLUMINESCENCE AND THERMOLUMINESCENCE OF UNDOPED LTB AND LTB:A (A = Cu, Ag, Mn)

THESIS

Zachary L. Hadfield, USA

AFIT-ENP-13-M-13

DEPARTMENT OF THE AIR FORCE
AIR UNIVERSITY

AIR FORCE INSTITUTE OF TECHNOLOGY

Wright-Patterson Air Force Base, Ohio

AFIT-ENP-13-M-13

CATHODOLUMINESCENCE AND THERMOLUMINESCENCE OF UNDOPED LTB AND LTB:A (A = Cu, Ag, Mn)

THESIS

Presented to the Faculty

Department of Engineering Physics

Graduate School of Engineering and Management

Air Force Institute of Technology

Air University

Air Education and Training Command

In Partial Fulfillment of the Requirements for the

Degree of Master of Science in Nuclear Engineering

Zachary L. Hadfield, BS

Major, USA

March 2013

AFIT-ENP-13-M-13

CATHODOLUMINESCENCE AND THERMOLUMINESCENCE OF UNDOPED LTB AND LTB:A (A = Cu, Ag, Mn)

Zachary L. Hadfield, BS
Major, USA

Approved:

Robert L. Hengehold, PhD (Chairman) — 14 Mar 2013 — Date

John W. McClory, PhD (Member) — 14 MAR 2013 — Date

LTC Stephen R. McHale, USA (Member) — 14 MAR 2013 — Date

Abstract

The Department of Defense is interested in lithium tetraborate ($Li_2B_4O_7$) crystals for their possible use as a solid state neutron detection material. With large concentrations of ^{6}Li and ^{10}B, it has a high neutron capture cross section. Furthermore, the crystal fluoresces in the presence of ionizing radiation, making it an attractive candidate for a scintillating detection device. However, there is a lack of fundamental knowledge about the material characteristics, particularly with regard to its fluorescent spectrum.

Cathodoluminescence measurements were conducted on undoped and doped samples of lithium tetraborate in order to characterize the nature of its fluorescent spectra under different environmental conditions. Measurements were made using a vacuum ultraviolet cathodoluminescence system specifically designed to detect high energy photons emitted in wide band gap materials. The cathodoluminescent spectra from 10 K to room temperature was characterized for six different lithium tetraborate crystals: three undoped crystals and one each doped with silver, copper, and manganese.

Thermoluminescence measurements were conducted using a Harshaw Model 3500 Manual TLD Reader. After electron irradiation from the cathodoluminescence experiment, the samples were heated from 50℃ to 250℃ at a heating rate of 1℃ per second. The thermoluminescence measurements provided insight into the carrier trapping ability of the crystals after electron irradiation.

Acknowledgements

This experiment would not have been possible without efforts from a vast number of people. I would like to thank my advisor, Dr. Robert Hengehold for his continued support and guidance throughout the course of this experiment. His vast understanding of the physical properties of the experiment and the cathodoluminescence system was invaluable. I would also like to thank Greg Smith for his countless hours of assistance in the lab. This work would not have been possible absent his practical knowledge of vacuum systems and their various components. I would like to thank the two members of my committee, Dr. John McClory and LTC Stephen McHale for their leadership and guidance. They provided the purpose and direction necessary for me to understand and pursue solutions to the problem. I would like to thank MAJ Mike Lee and Mr. Vincent Richardson for their assistance and teamwork in preparing the lab for this experiment. Lastly, I would like to thank all the members of AFIT and WPAFB whom I did not directly work with, but were no less instrumental in making this research a reality.

Table of Contents

List of Figures

Page

List of Tables

Page

CATHODOLUMINESCENCE AND THERMOLUMINESCENCE OF UNDOPED LTB AND LTB:A (A = Cu, Ag, Mn)

I. Introduction

1.1 Motivation

In an increasingly asymmetric battlefield environment, the threat of non-nation state nuclear proliferation activity drives the need to detect and interdict the transport of Special Nuclear Material (SNM) and nuclear devices. Globalization has opened new pathways to move SNM across national borders through shipping containers and cargo vehicles. Monitoring these containers is a monumental task due to the sheer number moving in and out of ports of entry every day. An inexpensive, yet effective means of detection is absolutely critical in order to deny the transit of SNM through ports of entry.

Detection can be accomplished with several techniques. Spontaneous fission of nuclear material and the subsequent decay of its daughter products give specific detectable signals. Of these signals, x-ray, beta, gamma, and alpha radiation are easily shielded, making detection difficult. Neutron radiation, however, requires different shielding materials, making it an attractive candidate for detection. The window for detection realistically lies between the time a container is placed on a ship to when it leaves its particular port of entry. Ideally, redundant systems would be emplaced to take advantage of this full window to maximize the chance of discovery.

Currently, neutron detectors are large gas systems, and must be fixed at hard sites at ports of entry or on ships. This constrains neutron detection to the containers next to

the fixed systems on ships, leaving most of the containers unchecked. At ports, this limits detection to a very small window of time as a container moves past a detector, reducing the probability of detection. A handheld, solid-state device could drastically increase the flexibility in employing neutron detection systems, thus increasing the probability of interdicting SNM moving into the country.

Lithium tetraborate (LTB), $Li_2B_4O_7$, is a crystal that contains lithium and boron isotopes, each with high probabilities of interacting with neutrons via nuclear reactions or elastic scattering. The fluorescent and thermoluminescent (TL) properties of LTB could provide a mechanism to detect both instantaneous and time-integrated interactions with neutrons. Exploration into the properties of LTB could result in fielding reliable, inexpensive solid-state neutron detection devices for use by the Department of Homeland Security to detect and interdict the transit of SNM into the United States.

1.2 Research Topic

In order to characterize LTB with various dopants and in both crystalline and glass form, several investigative techniques have been, and are currently being used. Electron paramagnetic resonance (EPR) and electron-nuclear double resonance (ENDOR) are being used to examine the nature of paramagnetic defects observed in crystalline samples [1-3]. X-ray diffraction has been used to validate crystal structure and quality [4]. Various types of luminescence, to include thermoluminescence, cathodoluminescence, and photoluminescence have been periodically used to observe the radiative relaxation spectrum of both crystal and glass samples [5,6]. Each of these techniques is subject to constraints and can only characterize the defect states they were

designed to detect. For example, EPR defect states must be paramagnetic while luminescent techniques are unable to characterize non-radiative relaxations.

The primary goal of this research was to use cathodoluminescence and thermoluminescence techniques to characterize undoped LTB and LTB:A (A = Ag, Cu, Mn) single crystals. Though cathodoluminescence spectra has been previously collected on LTB, the data are incomplete. Very little data exists for emissions of photons above 6 eV. This is due to the difficulty of propagating photons in the vacuum ultraviolet (VUV) energy range through the atmosphere or windows common to these systems, making VUV cathodoluminescence systems less common. Since LTB has a band gap of ~ 9.5 eV [7], VUV emissions are possible, opening the door to further research into this region of the emission spectrum. We constructed a system capable ofdetecting VUV photons by keeping photons emitted from a sample entirely in vacuum until they are detected by a PMT. Details of the experimental setup can be seen in paragraph 3.1.1 of this document. Thermoluminescence has also been done, but is generally completed after x-ray irradiation. The type of ionizing radiation will change the fill probability of various carrier traps, and TL has not been conducted after electron irradiation. Electron irradiation is qualitatively different in that it will fill all trap levels in a wide band gap material, something not easily achieved via laser or x-ray tubes. Research into this area is necessary to determine if electron radiation alters carrier trap fill ratios as opposed to other types of ionizing radiation.

1.3 Research Objective

The goal of this research was to characterize the fluorescent behavior of lithium tetraborate under previously untested conditions. High energy emissions above 6 eV

have not been previously detected in any research on the material thus far. Furthermore, data near liquid helium temperatures has not been investigated as well. This objective of this effort was to construct and use a system that was able to detect photons from 2-10 eV while irradiating an LTB sample with electrons. This would be sufficient to capture the band gap transitions (~ 9.5 eV) within the crystals, should they occur. Furthermore, the system was constructed to operate with liquid helium, allowing investigation at extremely low temperatures (~10 K).

Thermoluminescence data for LTB samples following electron irradiation are very sparse. Thus, after electron irradiation, thermoluminescence data were to be taken via the Harshaw TLD Reader at building 470. The resulting data would demonstrate the ability of the crystal to trap carriers with all states being filled through the electron ionizing radiation.

1.4 Crystal Fabrication

The LTB single crystals were grown from stoichiometric melt using the Czochralski method from platinum crucibles in air. Silver doping was done by adding $AgNO_3$ to the melt during solid-phase synthesis, while CuO is used for copper doping and MnO_2 was used for the manganese doped sample. A solid seed crystal was rotated and simultaneously pulled out of the melt to form large cylindrical shaped crystals. After cleaving, grinding, and polishing, the near-surface broken layer depth generally reaches ~ 50 nm [5,6]. This is important in CL experiments since surface states can significantly alter the nature of the emission spectrum. One must ensure the electron beam penetrates through the surface layer to the bulk of the crystal.

Advantages of the Czochralski technique are that the growing boule is not in contact with the crucible and the boule may be viewed during the growth run, making controlling the process easier. However, the main disadvantage is possible contamination of the melt by the crucible material. Since platinum crucibles are used, platinum and iridium (an element typically mined with platinum) are common impurities in the LTB crystal when this technique is used [8].

1.5 Samples

Figure 1-1: This undoped sample was grown in the Ukraine and part of the first batch AFIT received from this group. The sample was generally clear before irradiation.

Figure 1-2: This undoped sample was grown in the Ukraine and recently received at AFIT in an updated batch. The crystal was generally clear and uniform prior to irradiation.

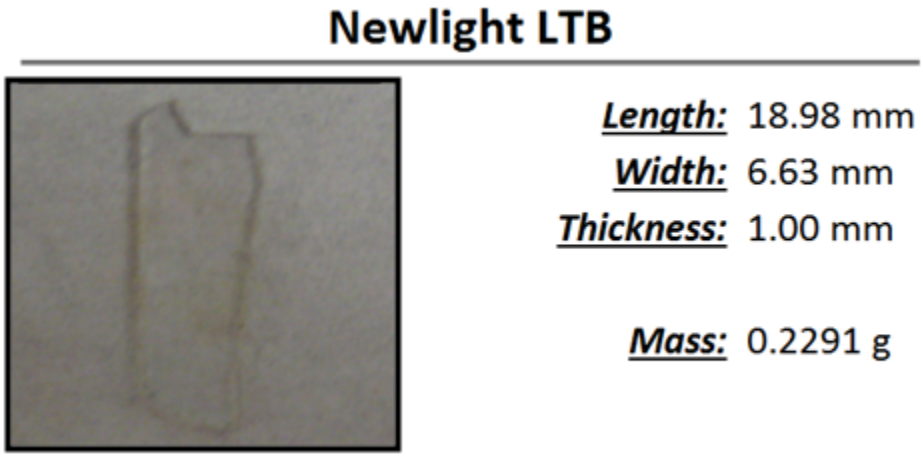

Figure 1-3: This sample was purchased from Newlight. Little is known about its growth technique. It was originally a part of a larger disc. The sample was extremely clear and transparent prior to irradiation.

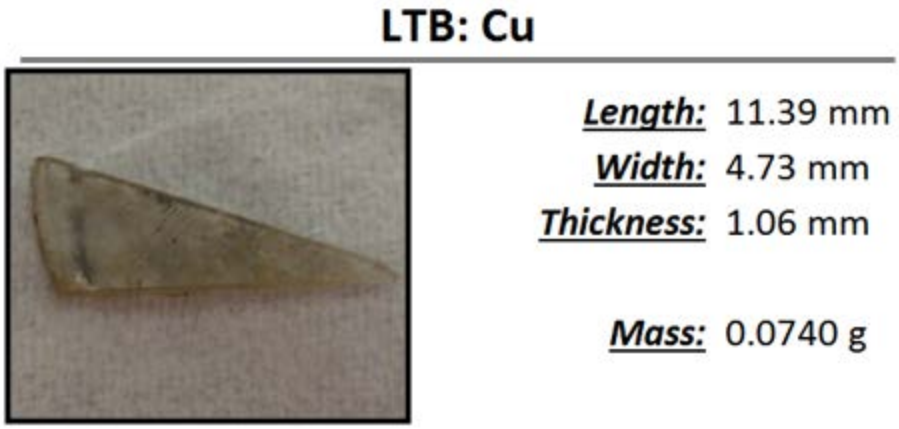

Figure 1-4: This copper doped sample was grown in the Ukraine and received in the 2nd batch that AFIT received. It is doped with 0.015% Cu and was generally clear prior to irradiation.

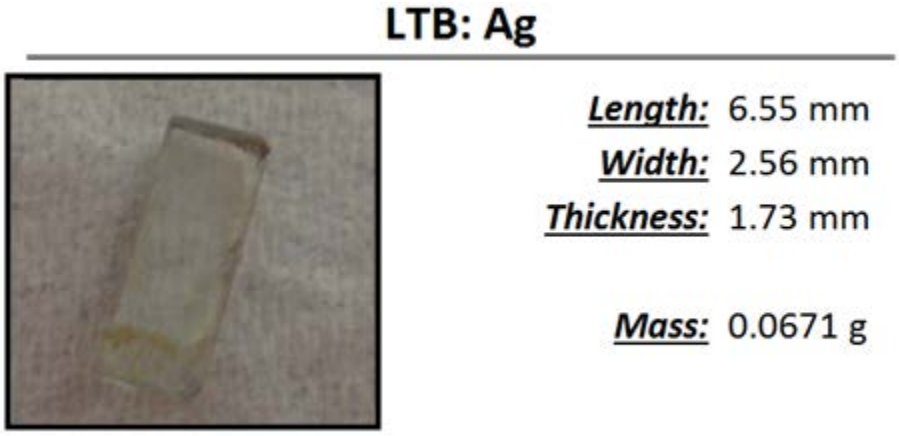

Figure 1-5: This silver doped sample was a part of the 1st generation of crystals from the Ukraine. Its doping concentration is unknown.

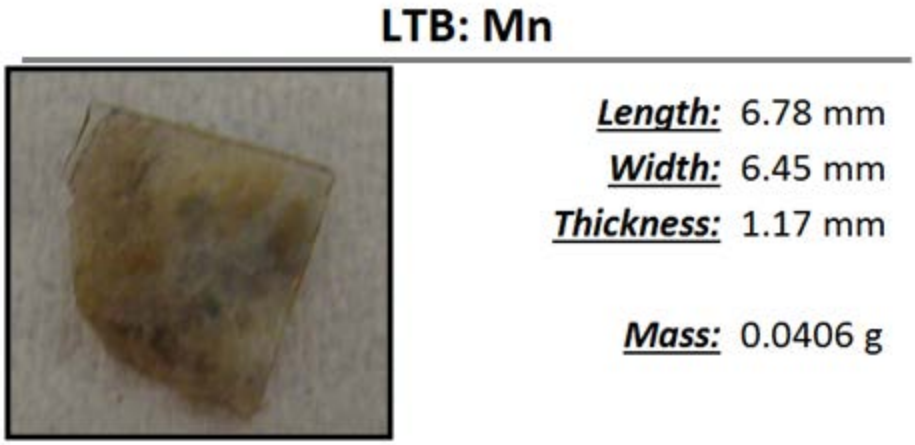

Figure 1-6: This Mn doped sample was from the 1st generation of crystals from the Ukraine. It is doped with 0.02% Mn and was the sample used in previous research.

II. Theoretical Background

This section explains the theory behind cathodoluminescence, thermoluminescence, and how they specifically relate to LTB.

2.1 General Properties of LTB

Lithium tetraborate is a tetragonal crystal in the space group $I4_1cd$ with lattice constants $a = b = 9.475$ Å and $c = 10.283$ Å at room temperature. It has a 104 atom unit cell (eight formula units) and a repeating $(B_4O_9)^{6-}$ basic anionic structural component, which consists of both BO_4 and BO_3 subcomponents. Each oxygen atom covalently bonds to two boron atoms and each lithium atom has five neighboring oxygen atoms [9]. Therefore, LTB is a rigid anion sublattice, seen in Figure 2-1, formed by the boron-oxygen network linked in a spiral axis of 4I symmetry. Within the sublattice are the weakly bonded lithium atoms aligned in the [001] direction, which charge compensate the crystal during growth. The lithium atom donates an electron to the B-O anion subcomponent, slightly polarizing the crystal. The B-O component becomes a negatively charged point defect that traps holes, while the lithium ion becomes a positively charged point defect able to trap electrons [5].

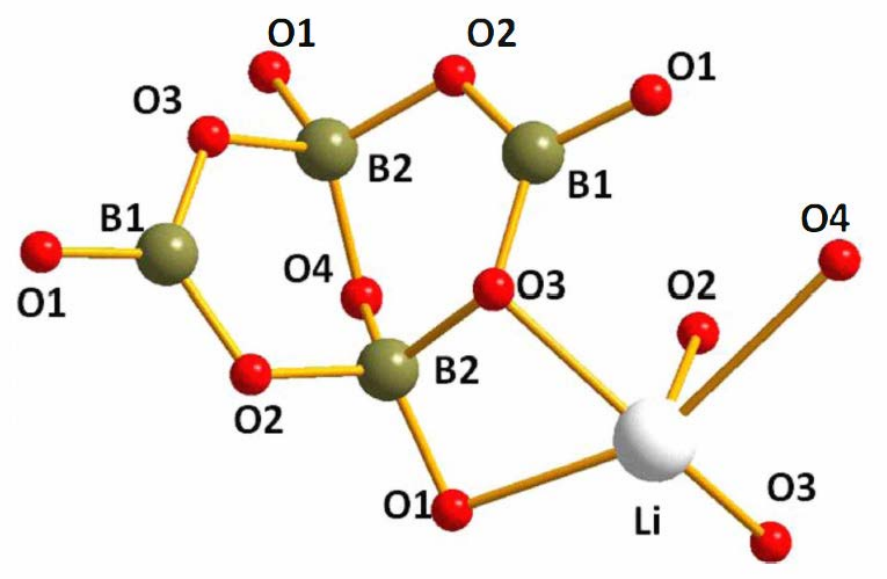

Figure 2-1: The main structural component of the $Li_2B_4O_7$ crystalline lattice. The B_4O_9 subcomponent has four boron atoms in two different lattice positions and nine oxygen atoms in four inequivalent positions. The lithium atoms are all equivalently positioned between the negatively charged B-O complexes and charge compensate the crystal. The O1 atoms depicted also belong to adjacent B_4O_9 components.

The energy band structure has been depicted in an article by V.T. Adamiv [10]. The valence band consists of the 2s-O, bonding BO_3, and bonding BO_4 orbitals. The bonding BO_4 complexes, formed by the two boron atoms in the tetragonal configuration, form the top of the valence band and displays significant dispersion. The antibonding BO_3, antibonding BO_4, and LiO_4 orbitals construct the density of states in the conduction band. The antibonding BO_3, formed by the two boron atoms in the trigonal planar configuration, create the bottom of the nearly dispersionless conduction band. The octahedral configured lithium atoms, LiO_6, produces an additional high energy band not depicted in this figure [10]. As seen in the diagram, a highly dispersive valence band edge and comparatively minimally dispersive conduction band edge make lithium tetraborate an insulator for holes and strongly correlated electron semiconductor [7].

Islam et al. from Germany attempted to theoretically calculate the band gap with widely varying results ranging from 6.2 eV to 17.68 eV with a best estimate at 9.0 eV after adjusting for a correlated system [11]. Using a combination of photoemission spectroscopy and inverse photoemission spectroscopy, David Wooten experimentally determined the band gap in four different crystal orientations with results ranging from 8.9 eV to 10.1 eV [7].

2.2 Thermoluminescence

Thermoluminescence (TL) is the process of heating a material, post irradiation, and observing emitted photons. The temperature at which photons are emitted correlates to the energy level at which carriers are trapped due to the previous irradiation. This correlation can be simply calculated using the Randall and Wilkins approximation to estimate the thermal activation energy associated with an observed TL peak and is given by

$$E \approx 25kT_m \tag{1.1}$$

where T_m is the peak temperature and k is Planck's constant [12].

The TL mechanism in LTB:A can be explained in the following way. During irradiation, an electron-hole pair is formed. The electron, now in the conduction band, is captured by an A^+ ion, creating an A^0 center. Conversely, the hole will be trapped in a hole trapping center on the boron-oxygen network. When the sample is heated, the trapped hole is released from the anion complex and becomes a free carrier. As it approaches the A^0 center, the trapped electron tunnels to an excited energy level around the hole, forming a small polaron followed by formation of an self-trapped exciton (STE) in an excited state [13]. They STE eventually radiatively decays at around 3.6 eV. This

explains why the TL spectrum of LTB:A radiates at the wavelength of the STE peak observed during cathodoluminescence experiments.

It is known that LTB: Cu creates a bimodal emission distribution centered at 128˚ C and 228˚C, corresponding to trapping levels of 0.7 eV and 1.4 eV, respectively [14]. The mechanism for the TL spectrum for LTB:Cu is as follows.

Boron has three electrons in its valence shell. The two boron atoms in the tetragonal configuration each borrow one electron from one of the cations located within the crystal to compensate charge. This modifies the anion network, making it a negatively charged point defect able to trap holes. Conversely, oxygen vacancies create positively charged point defects able to trap electrons. Furthermore, due to the mobility of the cations at room temperature, cation clusters can form, producing additional electron trapping centers [14].

Copper may exist in the $Cu^{0,+1,+2}$ oxidation states when used as a dopant. Since the atomic radius of copper (1.35 Å) is similar to that of lithium (1.45 Å), the majority of the copper doping atoms can act as a substitutional for lithium inside the crystal while the rest are positioned as interstitials. Copper will not substitute for boron due to boron's relatively small atomic radius (0.16 Å).

It follows that the substitutional copper atoms will create electron traps with higher thermal stability relative to the Cu^{+} ions positioned in the interstitial sites. The trapped electrons are released and subsequently radiate when the temperature is high enough to overcome their trapping energy. This is confirmed by experiment as the position of the 228˚C peak does not change with dopant concentration. The intensity of

this peak, however, does change with dopant concentration due to the larger number of lithium replacements and formation of high temperature electron trapping centers.

Conversely, copper atoms positioned in the internodal regions will occupy a wide variety of positions due to the complexity of the LTB crystal. Thus, increasing the dopant concentration changes the distribution of these positions and their ability to interact with each other. Thus, one expects the position of the low temperature peak (128˚C) to shift with dopant concentration, which is, in fact, observed [14]. The thermal stability of the low temperature peak decreases significantly with increasing dopant concentration.

Silver doped LTB, on the other hand, has only one observed peak at 160˚C [9]. Silver also has an atomic radius (1.65 Å) similar to lithium, and also exists in the 0,+1, and +2 oxidation states, like copper. It follows that silver atoms will also position themselves as substitutionals at the lithium lattice sites, while others are positioned as interstitials. One would then assume that silver would have two TL peaks. This discrepancy can be explained with three different possibilities.

Since the lower limit of the TL analysis was room temperature, one possibility is that the lower temperature peak corresponding to the silver interstitials is thermally unstable at room temperature, and the observed peak at 160˚C corresponds to the substitutionals. The 2nd possibility is that the high temperature peak is outside the temperature range analyzed (250˚C) and the observed peak corresponds to the interstitials. The last possibility is that the electron trapping levels of the interstitials and substitutionals are very close and unable to be resolved through thermoluminescence.

2.3 Cathodoluminescence

Cathodoluminescence (CL) is a phenomenon whereby electrons are accelerated and subsequently impact and excite a luminescent material. As the material relaxes back to its ground state, it emits photons which have energies corresponding to its radiative decay pathways. An analysis of the energy spectrum of the emitted photons gives insight into the quality and composition of the material. It is a very useful tool for investigating wide band gap materials due to the difficulties of propagating laser light through the atmosphere at the wavelengths necessary to produce free carriers.

Cathodoluminescence experiments can only observe final radiative decay of electronic transitions. There are a number of non-radiative crystal relaxation mechanisms that are undetectable with CL systems and need different types of experiments to observe and understand. Therefore, CL is only one piece of the puzzle in crystal characterization rather than a holistic approach to interpreting the behavior of solid state materials.

2.3.1 Electron-Beam Interactions in Solids

Energetic electrons interact with solid materials in two primary ways: ionizating and non-ionizing energy loss (NIEL). Ionization occurs when the incident electrons interact with bound electrons in the material and transfer enough energy to strip the electrons from their associated nuclei, creating free electrons. The newly freed electron subsequently releases its energy as it relaxes into lower energy forms through lattice vibrations, light, or electric current. The major element of non-ionizing energy loss is atomic displacement through elastic scattering and is the primary damage mechanism in electronic solid state devices. The displaced atom is called a primary knock-on atom (PKA) and can displace further atoms in a displacement cascade. However, kinematics

dictates that there are thresholds of energy that incident particles must have to overcome the displacement energy, E_d, of the target atom, which is usually on the order of 10 eV. Since electrons are very light particles in comparison to atomic nuclei, they cannot transfer much of their energy and still conserve momentum. Therefore, the threshold energy for incident electrons is typically on the order of 100 keV in order to displace atoms from their lattice locations [15]. The goal of cathodoluminescence is to be a non-destructive investigative tool, and energies for this experiment did not exceed 8.5 keV, far below the energy required to cause displacements.

Therefore, the incident electrons undergo ionizing energy loss (IEL) through ionizing atoms in the crystal, creating electron-hole pairs. The free carriers can be highly mobile depending on the material. Oxides, such as LTB, generally have low free carrier mobility, depending on the effective mass of the carriers. In LTB, holes have a very high effective mass, reducing their mobility and increasing their trapping rate. Electrons, on the other hand, have a moderately low effective mass, making LTB a free electron semiconductor [15,7]. Electrons can still be trapped on positively charged point defects, but the lifetime of these traps is small in comparison to the hole traps.

Since LTB is a wide band gap dielectric material, the nature and effects of charge trapping are quite diverse. It is a covalent compound of several elements and possesses a wide gap between its valence and conduction bands, hence a large variety of trapping energy levels are possible. Shallow hole trapping levels, a fraction of an eV above the valence band, are possible and permit holes to perform a random walk through the oxide, moving from trap to trap. This effect is stimulated in the presence of an electric field, a common occurrence in a material to be made into a device. However, deep traps can also

exist, trapping the holes for a very long time. Thermal processes and electric fields are very unlikely to liberate carriers from these traps, creating a pseudo-permanent array of trapped charge [15].

Upon excitation by the electron beam, the bulk of the material will contain both shallow and deep carrier traps, of which the fill probability will depend on the temperature of the material. At low temperatures, both shallow and deep trapping levels will be filled, reducing the amount of pathways for luminescence. However, at higher temperatures, carriers can be thermally excited from the shallow traps. If the shallow traps are not filled with carriers, they may provide a pathway for radiative relaxation that was not available at low temperatures.

If the crystal was grown in an oxygen-rich environment, oxygen excess centers can form such as the non-bonding oxygen hole center. If excess oxygen and hydrogen are present during the growth process, hydroxide (-OH) bonds can form in the lattice. Upon bonding with and trapping a hole, the oxygen releases its hydrogen atom. The hydrogen subsequently becomes lodged in the lattice and forms a permanent E' center and becomes an electron trap. Depending on its location in the lattice, the energy level of this trap can vary significantly [15].

2.3.2 Optical Colorability

Transparent materials, such as LTB, are clear due to their wide band gap. Optical photons, < 3 eV, are unable to excite carriers from the valence to conduction band, and hence the material is unable to absorb visible light. However, when exposed to radiation, transparent materials may darken as new energy levels are formed in the gap, creating color centers. The rate of colorability lies in the efficiencies of two primary steps:

forming a defect in a network or lattice and filling that defect with a hole or electron. It was previously established that the incident electrons used in this experiment do not have enough energy to cause displacements so the first criteria will not be changed due to this type of radiation. However, the thermal processing required to grow crystals with high-melting, strongly covalent materials leads to the formation of vacancies within the lattice. In LTB, this is particularly the case for oxygen vacancies, the most common defect in this crystal [7]. Therefore, defects are present in the crystal as grown, prior to any dose it receives in the experiment. Displacements are not needed to fulfill the first criteria of color center formation. The second criterion is fulfilled as the crystal responds to the ionizing dose it receives from the electron beam. Free carriers are produced and permitted to move about the crystal where they are trapped by these defects. The absorption power of the trapped carrier is determined by its quantum oscillator strength and can significantly vary depending on the nature of the defect [15]. If the oscillator strength is such that the carrier can absorb photons in the visible region, it will appear as coloring of the crystal to the human eye. Coloring of the crystals during the experiment may prompt investigation into the pre- and post-irradiation absorption spectrum of the material

2.3.3 Luminescence Processes in Solids

Luminescence from solids is typically attributed to impurities, excited state transitions of individual atoms, and lattice defects [16]. Luminescence processes compete with non-radiative processes to relax a solid upon excitation which include deep level impurities that trap carriers, Auger-related processes, and phonon coupling. Non-radiative processes tend to dominate transitions between closely spaced energy levels.

Shallow impurities consist of substitutional and interstitial dopants that create energy levels within the normal band gap of the material. Electron traps exist just below the conduction band while hole traps exist just above the valence band. Common oxidation states of an impurity generally determine if it is a donor or acceptor type dopant. Shallow impurity luminescence is generally observed at very low temperatures due to thermal ionization at higher temperatures [16]. Transitions that fall under this category include donor state to valence band, conduction band to acceptor state, or donor-acceptor pair (DAP) recombination. DAPs occur in compensated crystals and are a function of the distance between the electron and hole traps within the crystal involved in the transition. The emission energy of a DAP is given by

$$h\nu = E_g - (E_A + E_D) + \frac{q^2}{\varepsilon r} - \frac{q^2 b^5}{\varepsilon r^6}, \tag{1.2}$$

where q is the electronic charge, ε is the static dielectric constant, b is an adjustable Van der Waals parameter, and r represents the distance between the trapping sites [16]. DAPs generally emit a broad band luminescence spectrum due to the variation of r within the crystal. Furthermore, DAP peaks generally undergo blueshifts with increasing free carrier density, since more widely separated trapping sites saturate first [16]. Evidence of this behavior in a CL spectrum at low temperature is a clear indicator of a DAP transition.

Activators are dopants that generate luminescence through a slightly different mechanism than the shallow impurities. Radiative transitions take place between excited and ground states of the electronic levels of the impurity itself and not correlated to the host crystal. The impurity levels can exist within the band gap of a solid, and can be perturbed by the crystal environment directly surrounding the activator impurity [16].

Deep impurities are metastable carrier traps lying close to the center of the band gap. For this reason, they are generally thermally stable at room temperature and can trap carriers for long periods of time. Excitation from the ground state to excited states typically involves atomic displacements or phonons. Relaxation can be partially achieved through photon emission. If relaxation is primarily non-radiative, the impurity is referred to as a quencher [16]. Quenching impurities can drastically reduce the luminescent signal from an otherwise intensely radiative crystal.

Excitonic properties are intrinsic and correlated to the periodicity of the host crystal lattice [16]. Physically, an exciton is a Coulomb-coupled electron-hole pair. The relative strength of the Coulombic interaction determines the type and behavior of the exciton. Frenkel excitons are spacially small (on the order of a lattice constant) and characterized by strong Coulombic coupling between the electron and hole. Wannier-Mott excitons, however, are relatively large (several lattice constants) and have weak coulombic coupling. This allows them to move about the lattice, transferring the excitation as they go [16].

An excitonic state corresponds to an intermediate excited, yet unionized state of an atom within a crystal lattice. Thus, the energy of formation lies within the band gap [17]. The ionization energy, the energy corresponding to dissociating the exciton into free carriers, lies just below the conduction band and is given by

$$E_x = E_c - \frac{m^* q^4}{2h^2 \varepsilon^2 n^2}, \tag{1.3}$$

where m^* is the reduced effective mass of the electron and hole and n is an integer greater than or equal to one corresponding to the ground and excited states [16]. This allowed state within the band gap is not predicted with the Bloch model due to its failure

to incorporate Coulombic interactions between an excited electron and the hole it was excited from.

Excitons must have three conditions to form: low free carrier concentration to prevent Coulombic screening of the electron-hole interaction, small electric fields to prevent separation, and thermal energies below the ionization energy [16]. Frenkel excitons tend to form in high dielectric, large band gap materials where the reduced effective mass of the electron and hole is large. Conversely, Wannier-Mott excitons preferentially form in small dielectric, small band gap materials with a comparatively small reduced effective mass.

Bound excitons (BE) or self-trapped excitons (STE) also occur in bulk crystals when free excitons become bound to neutral and excited impurities, isoelectronic traps, and defects [16]. The energy levels can be described through the equation

$$E_n = E_g - E_x - \frac{E_B}{n^2}, \tag{1.4}$$

where E_B is the binding energy of the exciton [18]. A representation of these energy levels can be seen in Figure 2-3. Radiative emission of bound excitons occurs in the following way. A free exciton is formed or moves close to an impurity and becomes bound to it. The electron cascades down the exciton energy levels through the successive emission of phonons until it arrives at the lowest excitonic energy level, n = 1. If the ground state is still significantly above the top of the valence band, another decay mechanism is required to facilitate recombination. This generally occurs as radiative or Auger interactions [17].

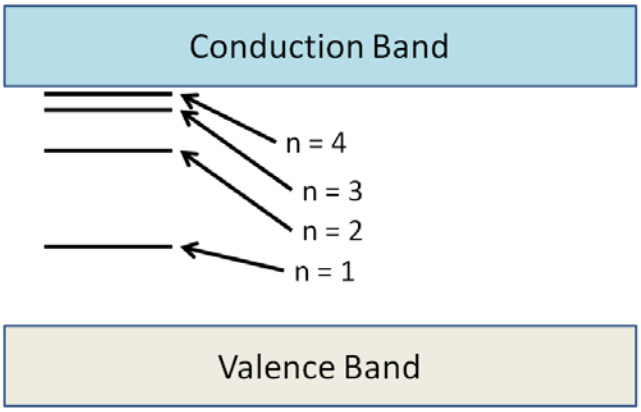

Figure 2-2: Energy diagram of excitonic energy levels within an insulator.

Therefore, one expects to see two forms of excitonic emission: direct radiative decay of free excitons known as edge luminescence and self-trapping luminescence corresponding to the ground state of excitons trapped near a perturbation in the periodic potential. Edge luminescence will occur at an energy

$$h\nu = E_x - E_V \,, \tag{1.5}$$

while self-trapping luminescence will correspond to

$$h\nu = E_{n=1} - E_V \,. \tag{1.6}$$

Edge luminescence will generally vary as a function of temperature, electric field, and free carrier concentration, while self-trapped luminescence will vary according to dopant concentration and crystal quality.

2.3.4 Non-radiative recombination mechanics

In the previous section, it was noted that luminescent relaxation processes compete with non-radiative processes. Though non-radiative relaxation mechanisms cannot be seen with CL, it is important to understand their characteristics because they will contribute to shaping or quenching the luminescent spectrum. The most prevalent

types of non-radiative recombination processes include phonon emission, Auger processes, and surface recombination.

Direct band to band phonon emission is extremely unlikely in insulators and most semiconductors due to the disparity between band gap and phonon energies. Simultaneous emission of over 100 phonons would be necessary for band to band transitions, which is extremely rare. However, as discussed before, phonons can be successively emitted through allowed excitonic energy levels, which explain the large Stokes' shift seen in solids like LTB [17]. Furthermore, due to the large number of defects, impurity types, and crystal configurations, these processes exhibit a broad band luminescent spectrum due to slightly different energies for the ground state excitons.

Auger processes are an important type of non-radiative recombination characterized by a three-bodied free carrier collision. As a hole and electron approach each other in real space, they can recombine, transferring their excess energy into kinetic energy of a nearby free carrier. If the nearby free carrier is an electron, it will be excited well above the bottom of the conduction band, at which point it can decay through successive phonon emission back to the bottom of the conduction band due to the large density of states in this region. Likewise, if the free carrier accepting the excess energy is a hole, it will drop below the top of the valence band and will recover back to this position in a similar fashion [17].

Surfaces of real materials possess additional defect states that supplement defect states present throughout the crystal, enhancing the recombination rate of free carriers at the surface. Furthermore, the surface states disrupt the periodic potential in different ways than the normal bulk defects, creating a larger variety of energy states within the

band gap. This affects both transition probabilities and the energetics of photon or non-radiative emissions [17].

2.3.5 Undoped LTB CL Characteristics

In order to facilitate the understanding of the cathodoluminescent behavior of LTB, the undoped behavior must first be examined. A very good insulator, LTB has the potential to emit photons ~ 1200 Å, corresponding to a full band gap radiative transition. A perfect undoped crystal would only radiate at this wavelength, but this is not observed in real samples due to defects and the peculiarities of LTB.

The most common bulk defects observed in undoped samples are oxygen vacancies, which modify the anion network [7]. Recall that oxygen atoms have four different positions within the lattice network. A vacancy in each of these positions will disrupt the lattice in slightly different ways. Perturbed vacancies can also exist, in which two or more vacancies occur within close proximity to one another, further compounding the variety of defects. Unfortunately, oxygen vacancies do not create states that prefer radiative transitions, and therefore cannot be directly observed with CL. Electrons existing in oxygen vacancy traps can tunnel to a nearby free hole, creating a small polaron. The polaron subsequently forms an STE in an excited state, and eventually decays radiatively at ~ 3.5 eV and can be seen in an article by V.T. Adamiv [6]. Therefore, oxygen vacancies can only be observed as a portion of the STE spectrum using CL.

In fact, nearly all defects in the LTB crystal behave in the same way with a few exceptions. A 2.2 eV (564 nm “Green”) emission has been previously observed [6]. The origin of this emission is attributed to an F type center induced by an oxygen vacancy and

is thermally unstable at room temperature. Therefore, the sample must be cooled to effectively observe this emission. This presents problems due to the difficulties of conducting CL at room temperature for LTB due to surface charging. Furthermore, this emission is dominated by the broad and intense STE spectrum, making it even more difficult to characterize. However, this emission is not seen nearly as readily with doped samples, so it is a competing process with transition metal activators.

Another emission has been reported at ~ 6 eV (207 nm "UV") [5]. Of unknown origin, this emission is most likely due to an allowed electronic transition created by a mid-band gap energy defect state. Data for the temperature dependence of this emission is sparse and is in need of characterization. Interestingly, both of these observed transitions are rather deep lying defect states (~ 2.2 eV and ~ 3.5 eV). This indicates that the probability of an electron tunneling from its defect trap to a nearby self-trapped hole decreases with the increasing potential barrier it must overcome, opening the door to a direct radiative transition to a lower energy state. Shallow trapping states below 2 eV, however, have not been radiatively observed in the CL spectrum. Applying the same logic, an electron in a shallow trapped state has a small potential barrier to tunneling to a nearby self-trapped hole, increasing the probability of this occurrence and thus decreasing the probability of radiative decay. Therefore, the shallow trapping states are only seen indirectly through the STE emission spectrum.

Data of emissions above 7 eV is extremely sparse, and it is one of the goals of this research to provide that data. Free exciton emissions at low temperatures are expected to be observed at energies just below the band gap. Full band gap transitions may be

observed as well, although it is not expected due to a forbidden quantum selection rule [19].

2.3.6 LTB: Ag

Silver doping of an LTB crystal will significantly alter the luminescent spectrum produced under electron irradiation. As previously stated, silver atoms will substitute for lithium atoms, creating a large quantity of Ag^+ ions within the crystal to balance charge. Ag^+ atoms are known activators and contain a $4d^9 5s \rightarrow 4d^{10}$ metal-centered electronic transition that has been shown to intensely radiate in LTB: Ag at 4.62 eV and can be seen in an article by V.T. Adamiv [6,20].

The familiar excitonic emission at ~ 3.5 eV is present, although its relative intensity to that of the undoped sample is diminished by ~ 50% [6]. This is an indicator that the previously mentioned electronic transition and radiative exciton emissions are competing processes. This makes sense since any incident electron that transfers energy to the Ag^+ electronic transition will not be able to use that energy to form excitons.

The 2.2 eV emission observed in the undoped LTB crystals is unresolved in LTB: Ag [6]. A slight asymmetry is observed on the low energy side of the 3.5 eV exciton peak, so the 2.2 eV emission may still be present, but at drastically reduced intensity. This is yet another indicator that the silver activator competes with the normal radiative decay mechanics of undoped LTB crystals.

2.3.7 LTB: Cu

Copper doping of an LTB crystal adjusts the luminescent spectrum in a somewhat more subtle way than the silver. Like silver, copper ions will substitute at the sites usually occupied by the lithium atoms. Furthermore, Cu^+, is also an activator that

undergoes a $3d^9 4s \rightarrow 3d^{10}$ metal-centered electronic transition. However, this transition is not as intense as in the silver doped sample and radiates at 3.40 eV, which is very close to the very broad and intense STE emission seen at 3.55 eV in LTB: Cu [6]. An article by V.T. Adamiv displays the nature of these emissions [6]. Note that the relative intensity of the activator emission is increased with respect to the STE emission at 80 K. This indicates that the activator is less dependent on phonon coupling in order to create the radiated photon.

2.3.8 LTB: Mn

The research into LTB: Mn is less extensive than the copper or silver doped samples, but it was addressed in MAJ Christina Dugan's thesis in 2011. The atomic radius of Mn is 1.79 Å and substitutes for at lithium sites during the growth process. However, unlike silver and copper, Mn only commonly occurs in the Mn^{+2} oxidation state. Therefore, when it substitutes for lithium, it creates a localized positively charged region, which can more effectively trap electrons than the lithium. As a more effective electron trap, higher concentrations of Mn result in a reduced mobility of electrons in the sample, somewhat skewing the normal effective mass ratios between carriers. This will change conductivity, but may not necessarily change the radiative spectrum of the sample. Other than some slight narrowing and blue-shifting of the peaks, very little change was observed in her analysis of the Mn doped sample in comparison to the undoped crystal [5].

Radioluminescence experiments using an X-ray tube on LTB: Mn was conducted by a Polish group in 2004. The results of this experiment can be seen in an article by D. Podgorska [21]. At room temperature, two large peaks occur at around 315 nm and 370

nm. These peaks are assigned to properties of the undoped LTB crystal itself and not from doping. However, the peaks at 430 nm and 610 nm are assigned to the Mn doping [21].

III. Methodology

3.1 Cathodoluminescence

3.1.1 System Setup

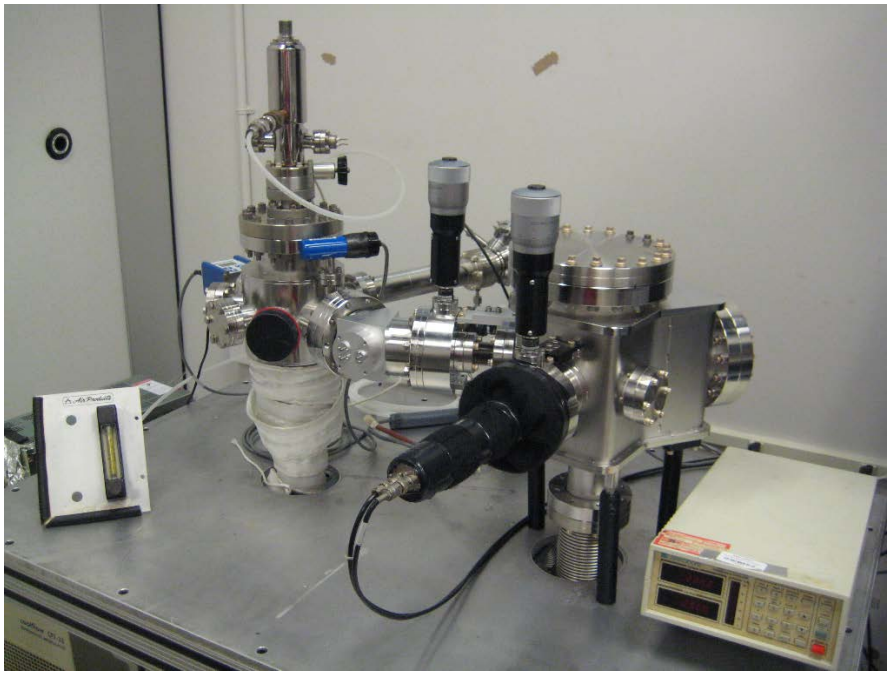

Figure 3-1: The VUV cathodoluminescence system in the CL lab at building 644. This system is unique in that light emitted from the sample travels through vacuum all the way until it is detected by the PMT. Therefore, high energy photons generally attenuated by the atmosphere or windows can be detected with this system.

This experiment used a system designed to take cathodoluminescence measurements and detect high energy photons emitted in the visible and ultra-violet regions: ~ 2-10 eV. The main feature of this system is that it keeps the photon signal emitted from a sample in a vacuum from the moment it is emitted to the time it is collected by a PMT. At no time does it pass through any windows or air at pressures above 10^{-7} torr. This is essential since photons from 6-10 eV are readily attenuated in the atmosphere and windows.

The VUV system setup, seen in Figure 3-2, consisted of an electron gun, cold finger, and monochromator mounted to a sample holding chamber. Attached on the back side of the monochromator was a photomultiplier tube. At the end of the cold finger was a copper mount, designed to optimize temperature control of the sample. A tantalum sample carrier was screwed into the copper mount with the sample held by tantalum wire spot welded to the carrier. This prevented the use of vacuum grease or other mounting materials that can condense onto the surface of the sample during irradiation. Liquid nitrogen or liquid helium could be fed into the cold finger to cool the sample, while a heater could monitor and set the sample at the desired temperature.

The electron gun was used to irradiate the sample, which would then fluoresce. Photons from the sample would diverge spherically, with some of them incident on the focusing mirror. The mirror focused the light onto the first slit of the monochromator. The light proceeded through the slit and onto the rotatable grating. The grating could be scanned or set into a fixed position in order to reflect the proper wavelength of light onto the second slit. After the photons passed through the second slit, they were incident on a layer of sodium solicitate, designed to convert ultra-violet photons into 400 nm photons detectable by the PMT. Finally, the PMT converted the incident 400 nm photons into electric signals.

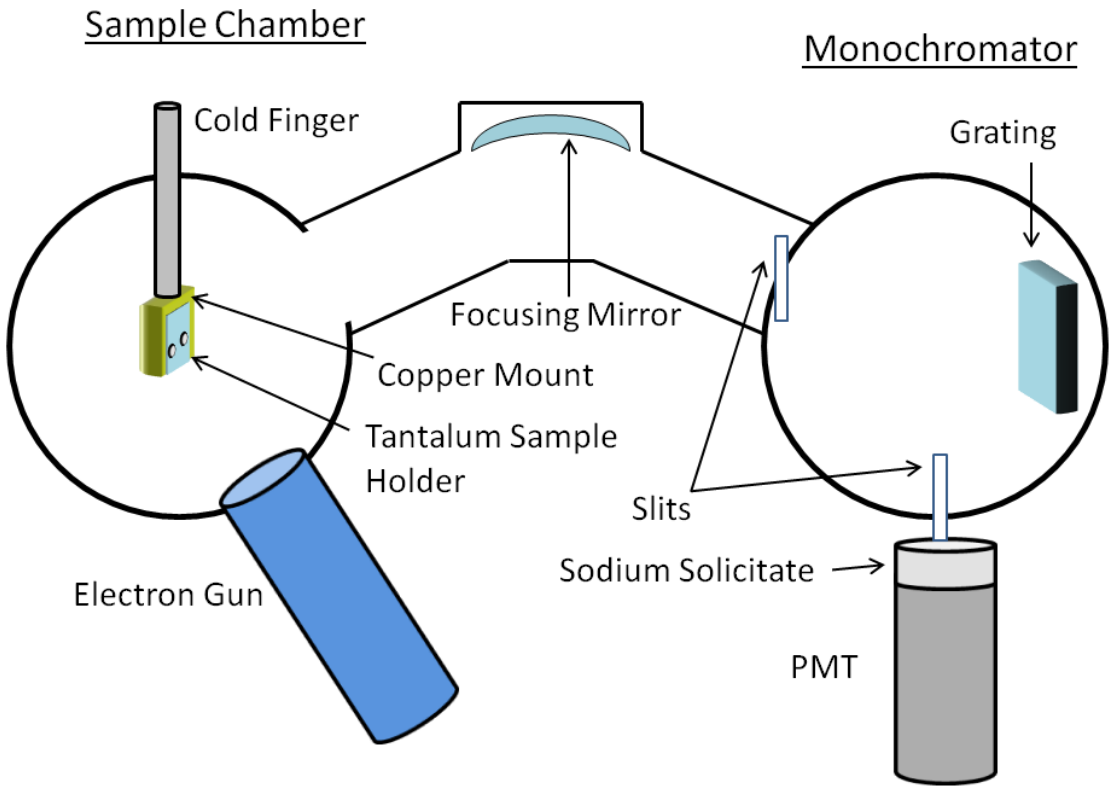

Figure 3-2: Diagram of the VUV experimental setup.

Electron Gun	Kimball Physics EMG 14
Monochromator	McPherson 234/302 UHV
Photomultiplier Tube	Hamamatsu R6094
Temperature Regulator	Lake Shore Model 330
Picoammeter	Kiethley Model 6485
Photon Counter	SR430 Multichannel Scaler

The VUV system was calibrated with a mercury lamp in order to test the accuracy and resolution of the spectrometer. The results can be seen in Figure 3-3. The spectrometer was determined to be accurate to within 0.5 nm with a resolution of 3 nm.

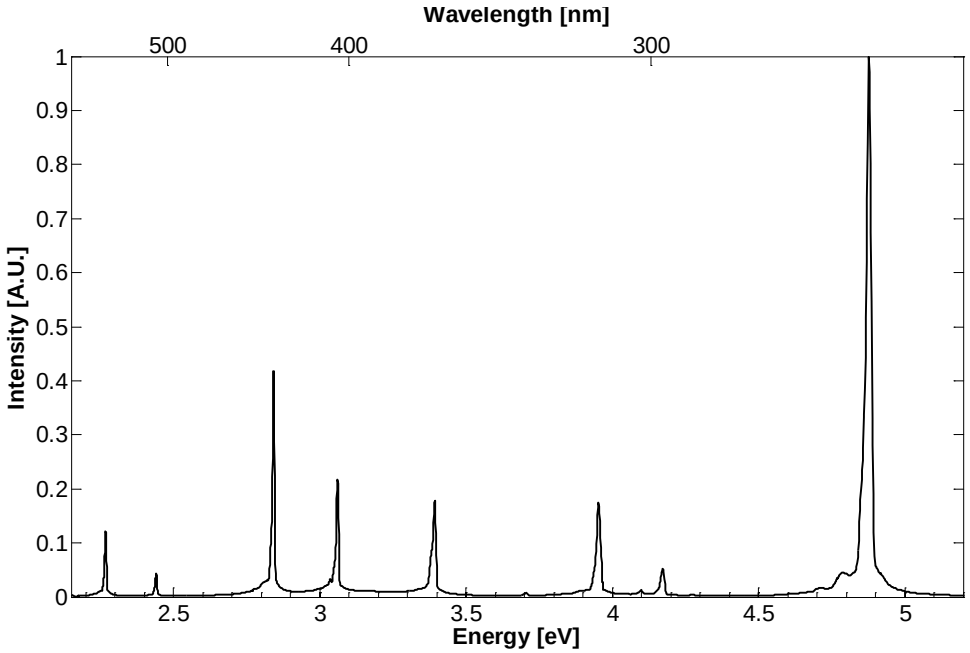

Figure 3-3: Mercury Lamp Calibration for the VUV spectrometer.

3.1.2 Electron Source

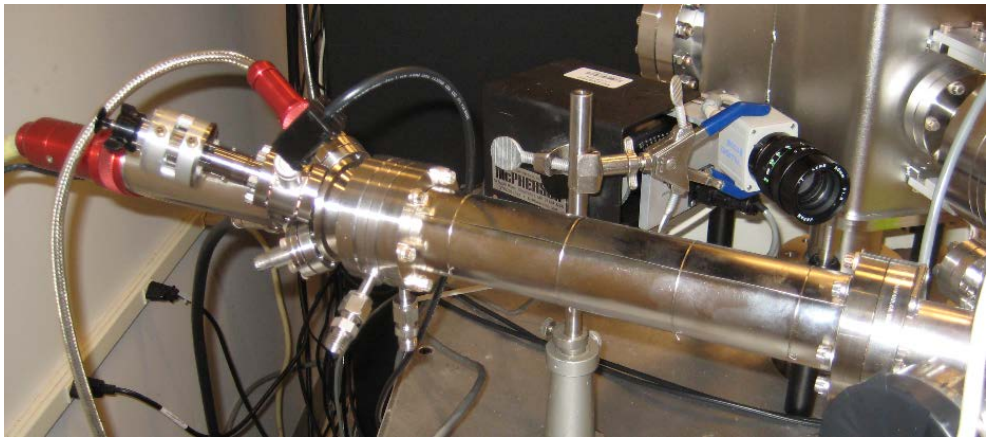

Figure 3-4: The Kimball Physics EMG-14 electron gun. This was used to accelerate electrons to the source.

The electron source for this experiment was a Kimball Physics EMG-14 electron gun. The electron gun passes a current through a refractory metal filament in order to evaporate electrons off the surface. The free electrons diffuse into the acceleration

region, where they are accelerated by a voltage difference to a user set energy (100 eV to 10 keV), forming the electron beam. The beam then passes by a series of deflector plates that can be used to change the trajectory or focus of the beam to optimize it for the experiment. A Faraday cup assembly is placed at the end of the apparatus and supplies a signal to a picoammeter, allowing the operator to measure beam current. The Faraday cup can then be moved out of the beam line to allow the beam to exit the gun and into the vacuum chamber. Beam current, divergence, energy, and deflection can all be adjusted over wide ranges. Furthermore, the electron beam can be pulsed with a beam blanker for timing applications. The electron gun receives an input signal, and subsequently applies high voltage to deflection plates near the exit of the gun, effectively pushing the electron beam off the target with a pulse width of 1μs [22].

3.1.3 Monochromator

The spectrometer used in this experiment was the McPherson Model 302 UHV Monochromator. It has a 0.2 meter focal length and is specifically designed to cover the wavelength region from 30 nm to 560 nm. It uses a spherical reflection grating with a resolution on the order of 1 nm. Though the spherical grating greatly reduces resolution, the spectrometer integrates into the vacuum chamber to avoid the need to pass VUV photons through a window or the atmosphere, where they are easily attenuated. This allows one to observe high energy radiative transitions in wide band gap materials, though at a cost of reduced resolving capability [23].

3.1.4 Photomultiplier Tube

The photomultiplier tube (PMT) used in this experiment was a Hamamatsu R6094, an 11 stage device with an electron gain of $2.1X10^6$. The range of spectral

response is from 300 – 650 nm with the wavelength of maximum response at 420 nm. Since this experiment was concerned with VUV photons, a layer of sodium salicitate was used to convert short wavelength photons to 400 nm, very close to the maximum response region of the PMT [24].

3.1.5 Photon Counting

Photon counting was done using the SR430 Multichannel Scaler/Averager. The SR430 counts incoming pulses in successive time bins with no dead time in between. The duration of the time bins is programmable from 5 ns to 10.5 ms with a maximum of 32,704 bins per record and up to 65,535 records per run. A trigger initiates each record whose data is summed or averaged to the bin by bin accumulation of all previous records. Timing information can be extracted due to the multichannel characteristics of the system, or the bins can be added together when timing is not considered. Furthermore, built-in discriminators allow one to program the photon counter to filter out noise occurring in the electronics. The SR430 is essential to the VUV system since it improves the signal-to-noise ratio and allows for precise statistics at each data point [25].

Figure 3-5: The Stanford Research Systems SR430 Multichannel Scaler/Averager. This component is designed to simplify time-resolved photon counting experiments, but proved invaluable for time-independent work as well.

3.2 Sources of Error

3.2.1 Thermionic Emission

The natural place to begin calculating error in the system is to observe background counts when the electron gun is completely off, isolating noise to that of the detector and the subsequent electronics. In order to minimize the background photons from exciting the photocathode of the PMT, the lights were turned off and ambient light was reduced to a minimum in the room. The PMT was covered with a dark cloth to prevent light from entering the system from the outside and a spectrum was taken. The results can be seen in Figure 3-6. With an integration time of 1 s per increment, the number of counts is level across all wavelengths with a mean of 5480 counts with a standard deviation of 174. Therefore, the background counts can be attributed to thermionic emission of electrons from the photocathode in the PMT, and not to any ambient light of a particular wavelength entering the system. This will introduce error into the experiment, but the error is equivalent across all wavelengths.

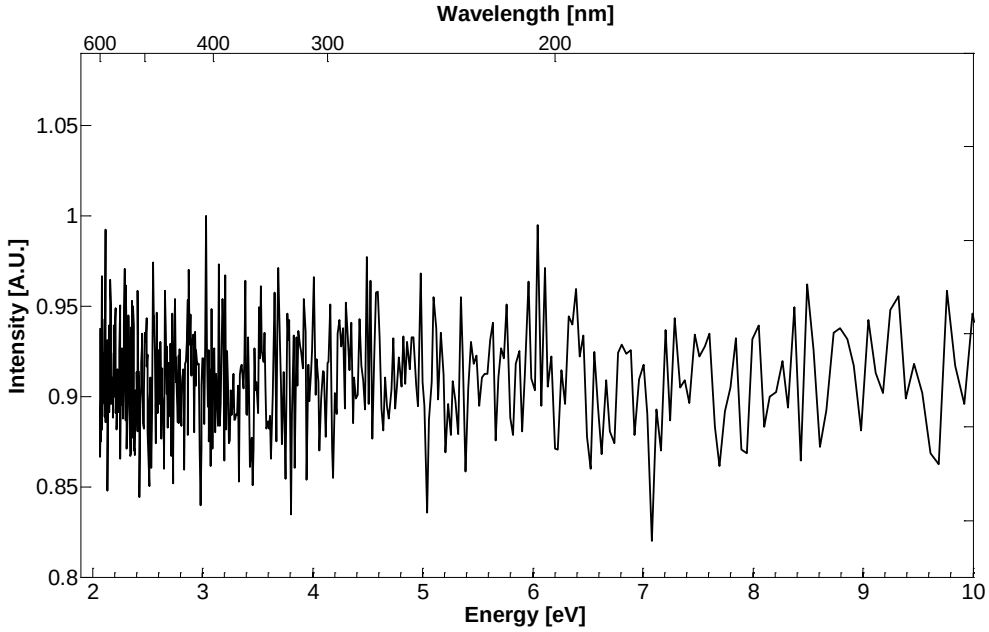

Figure 3-6: Background noise in the system when the electron gun is off. This noise, ~ 5600 counts per increment, primarily comes from thermionic emission from the photocathode of the PMT.

3.2.2 Filament Blackbody Spectrum and 0th Order Reflections

The next step was to turn on the electron gun and direct the electron beam off the sample. The sample was not excited, and thus gave off no emissions. A spectrum with 1 s integration time per increment was again measured as in the previous section and can be seen in Figure 3-7. The result was a Planckian distribution representative of blackbody radiation. This is attributed to the filament in the electron gun radiating as a blackbody. Its spectrum gets reflected off the sample and sample holder into the monochromator, creating the observed effect.

Near the short-wavelength limit of the grating (100 nm), the angle of the grating is such that the light from the incoming slit is directly reflected like a plain mirror to the exit slit since the angle of incidence equals the angle of reflection. In this region, the grating gives both the short-wavelength diffracted light and a reflection of all

wavelengths. Therefore, any light, regardless of wavelength, will contribute to the intensity in this region.

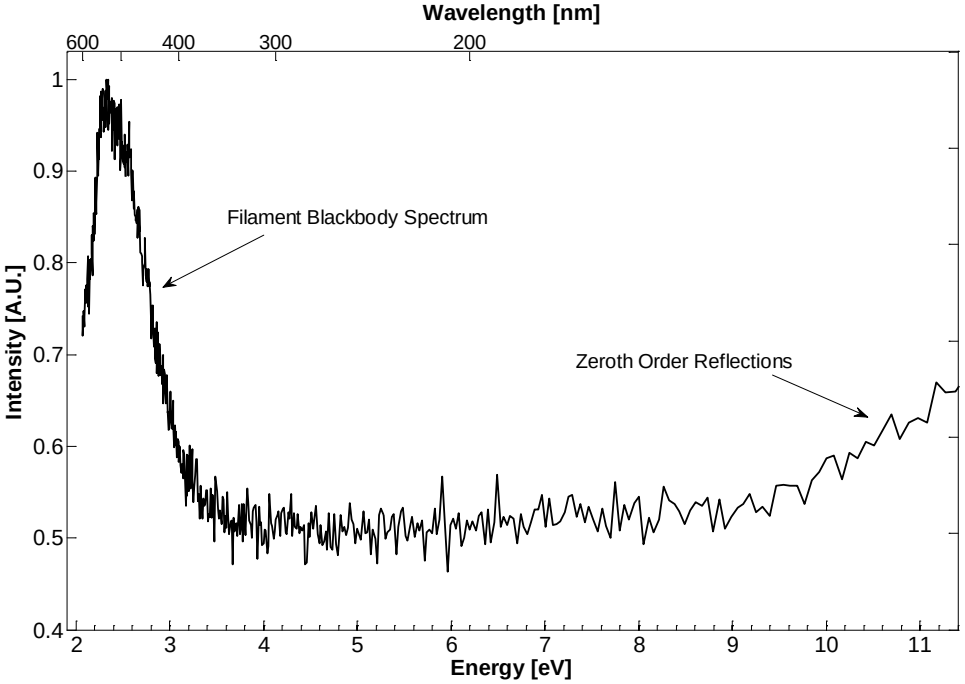

Figure 3-7: Background spectrum with the electron gun turned on, but with the electron beam not illuminating the sample. The low-energy background appears Planckian, and is assigned to the glow of the filament in the electron gun reflected off the sample. The high-energy background is due to zeroth order reflections off the grating. The baseline of the plot is at the level of the background when the electron gun is off.

3.3 Thermoluminescence

3.3.1 Experimental Procedure

Thermoluminescence was conducted on the six LTB samples after electron irradiation from the cathodoluminescence experiments. After the CL experiment was complete for a particular sample, the TL experiment was conducted. It took approximately one hour from the last electron irradiation to the beginning time of the TL experiment. This was mainly due to the fact that the CL system had to be evacuated and resealed prior to leaving the lab and the TL machine requires a 30 minute start up time in

order to allow nitrogen gas to cool the PMT inside the device. The samples were at room temperature during transport. The one hour time between irradiation and experiment start should have virtually no impact on experimental results. The lowest temperature the Harshaw TLD reader will begin taking measurements is 50℃. Defect states which are thermally destabilized at this temperature will have virtually zero thermal excitation of carriers out of their trapping sites at room temperature.

3.3.2 Harshaw TLD Reader

This experiment utilized the Harshaw Model 3500 Manual TLD Reader with WinREMS, a PC-driven, manually-operated, tabletop instrument for thermoluminescent dosimetry (TLD) measurements seen in Figure 3-8. It reads one dosimeter per loading and accommodates a variety of TL configurations such as chips, disks, rods and powder. The WinREMS software is a Windows-based dosimetry management system designed to track patient information. The reader uses contact heating with a closed loop feedback system to produce linear increasing temperatures accurate to within +/- 1℃ and with a range of 50℃ to 400℃. The reader uses nitrogen to flow around the sample to reduce oxygen-induced TL signals and to protect the PMT from moisture caused by condensation [26]. The main drawback of this system is that the data cannot be extracted from the software; it simply outputs the results on a screen display.

Figure 3-8: The system setup of the Harshaw Model 3500 Manual TLD in building 470.

3.3.3 Sources of error

The main sources of error for this system are the inconsistent thermal contact of the sample with the mounting area and the constraint of a 1 ℃/s heating rate. The mounting area on the reader is a metal plate with a slight recession approximately 6 mm x 6 mm. Consequently, if a sample is bigger than this, it does not fit squarely on the mounting bracket and thus reduces its thermal contact with the system. This will cause inadequate heating of the sample and skews the results. The sample can be moved to the side where it can sit squarely on the bracket with good thermal contact, but this could possibly reduce the intensity read by the PMT, again skewing the results. There is no good solution to fix this problem. However, for this experiment, the sample was placed off to the side for better thermal contact, owing to the idea that a sacrifice in intensity was preferred over inaccurate data on the temperature of the sample during an emission. In

other words, the position of the peaks as a function of temperature is more important than the absolute intensity of the emission. This stands to reason as little knowledge can be extracted by the absolute intensity of any recorded peak. The limitation of the heating rate further limits the accuracy of the results. If the heating rate is too fast, electrons or holes will not have sufficient time to excite out of their traps at a given temperature, causing them to emit at higher recorded temperatures than would be necessary to destabilize the defect state. This skews the data and overestimates the trapping energy of any given state.

IV. Results and Analysis

4.1 Monte Carlo Simulation of Electron Trajectory in Solids (CASINO)

4.1.1 5 keV in Undoped LTB

CASINO modeling using Monte Carlo simulations was used to determine the incident electron penetration depth, location, and energy deposition into an undoped sample of lithium tetraborate. The simulation parameters included a Gaussian shaped electron beam with a 20 nm beam diameter with 20,000 total electrons. The energy of the electrons was set to 5 keV, which was the primary energy used in the actual experiment. Figure 4-1 is a top-down view of electrons entering a crystal. The top of the graph is the point of entry. As the electrons erratically move through the crystal, the blue lines represent their paths of motion. A sense of how far they penetrate and how far they can move radially from the point of entry can be gathered. One observes a maximum radial displacement of +/- 350 nm from the point of entry. Therefore, when a beam is on a sample in the experiment, one can expect that it will deposit its energy close to the beam and not move laterally through the sample, throwing off alignment of the spectrometer. Furthermore, the maximum penetration depth lies at around 520 nm from the surface of the crystal. Since the crystal is thicker than 520 nm, no electrons pass through the crystal, which would be a source of energy not used to excite the material.

Figure 4-2 is a CASINO output that displays the maximum penetration depth from the 20,000 electron simulation. The shape is pseudo-Gaussian with an average depth of ~ 380 nm. The maximum depths nearly all occur between 57 nm and 560 nm from the surface. Figure 4-3 shows the energy deposited by the incident electrons into the crystal as a function of the radial displacement from the point of entry and the depth

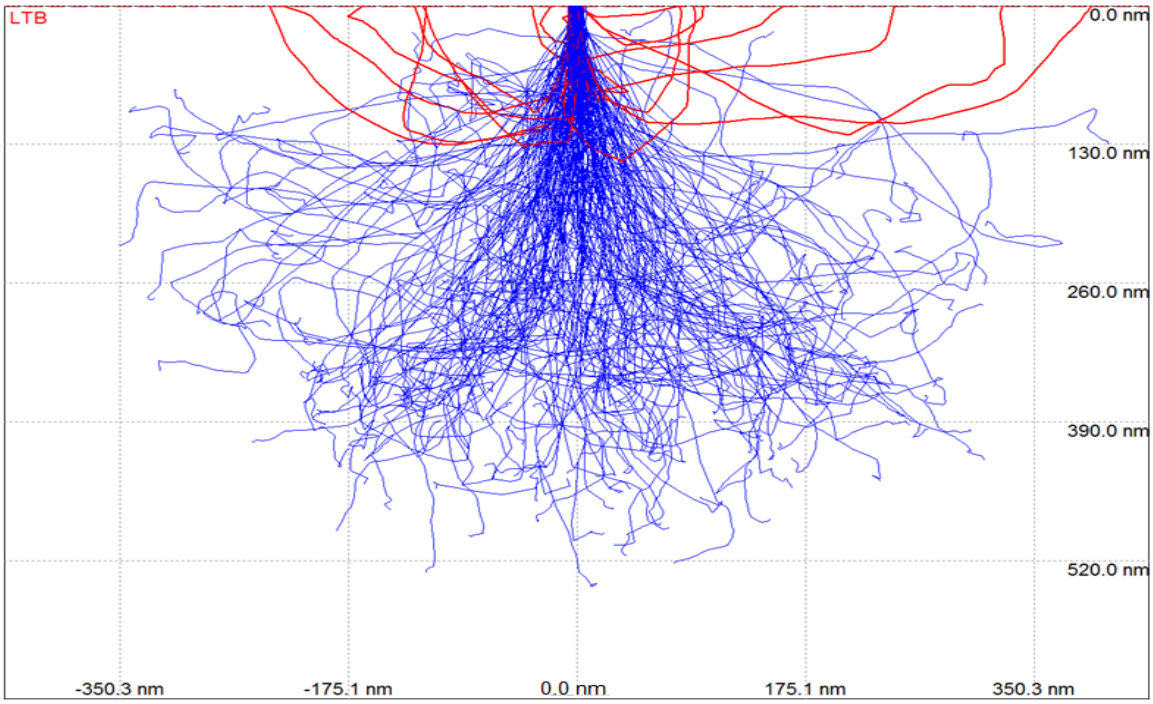

Figure 4-1: CASINO model results of electron penetration depth in undoped LTB with a 5 keV electron source emitting 20,000 electrons. The blue lines represent the paths of the incident electrons as they move through the crystal depositing energy. The red lines represent incident electrons that are backscattered out of the same surface they entered. These electrons only deposit a portion of their energy before leaving the crystal.

into the crystal. This data is important in the experiment since one needs to know how far in the surface of the crystal energy is being deposited. This will determine the likelihood of emissions resulting from surface states or bulk characteristics of the crystal. As a general rule, surface states exist within ~ 50 nm from the surface of a crystalline lattice. This is where the lattice deforms in response to the lack of additional atoms outside the surface to bond to the crystal and maintain its shape. The complex nature of this deformation typically results in an additional density of states that can form both radiative and non-radiative relaxation pathways from an excited to lower energy state.

As a result, the luminescent signature will appear different if the crystal is excited near the surface as opposed to the bulk.

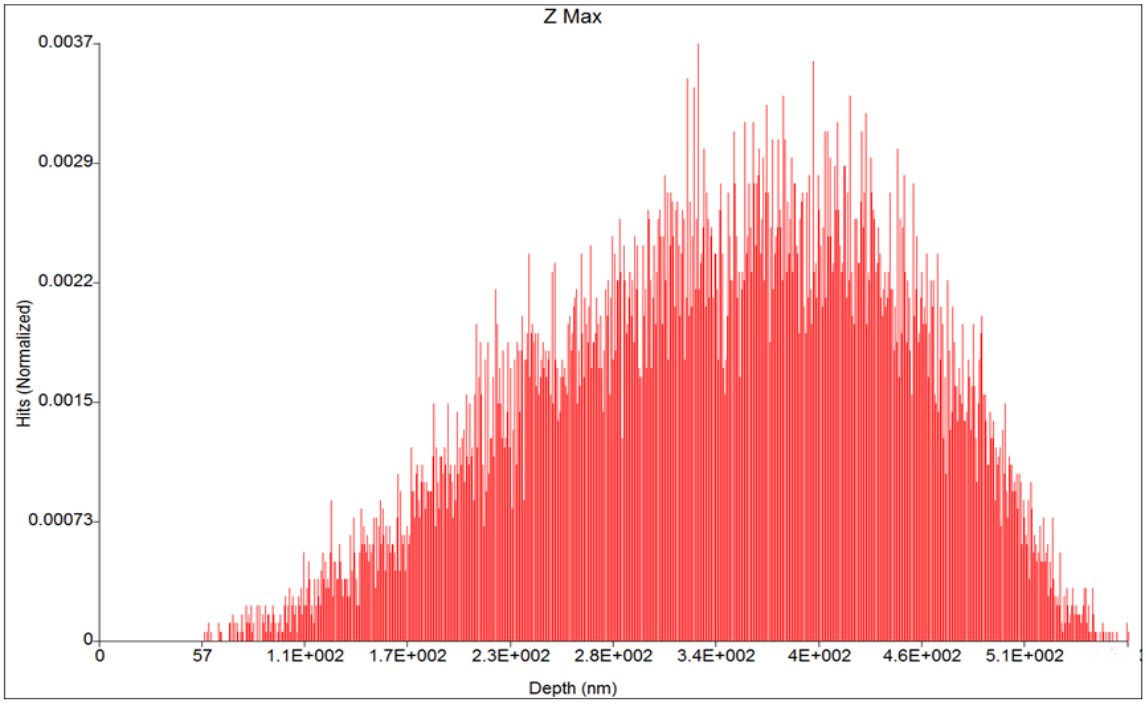

Figure 4-2: Maximum electron penetration depth in undoped LTB with a 5 keV electron gun source. The penetration depth distribution is pseudo-Gaussian with an average depth of ~ 380 nm.

Figure 4-3 clearly shows that with 5 keV electrons, the majority of the energy absorbed by the crystal is well within 50 nm from the surface. Therefore, the crystal will relax via its bulk density of states characteristics and give the associated spectrum. Since lithium tetraborate is comprised of low Z atoms, it has a fairly low electron density through which incident electrons can interact. In order to deposit energy near the surface, incident electrons around ~ 1 keV would need to be used. This presents practical problems. The lower the incident electron energy, the fewer collisions it will undergo before losing enough energy to become absorbed by its environment. Fewer collisions mean fewer free carriers liberated in the crystal to be available for radiative relaxation.

This means the luminescent signal will be drastically decreased. The beam current can be increased, but has a maximum recommended operating value before it becomes risky to burn out the filament in the electron gun. At 1 keV, with the beam current at its maximum value, the signal was too low to record any luminescent spectrum at all. Unfortunately, this constraint precludes the analysis of surface states in LTB with the current system configuration.

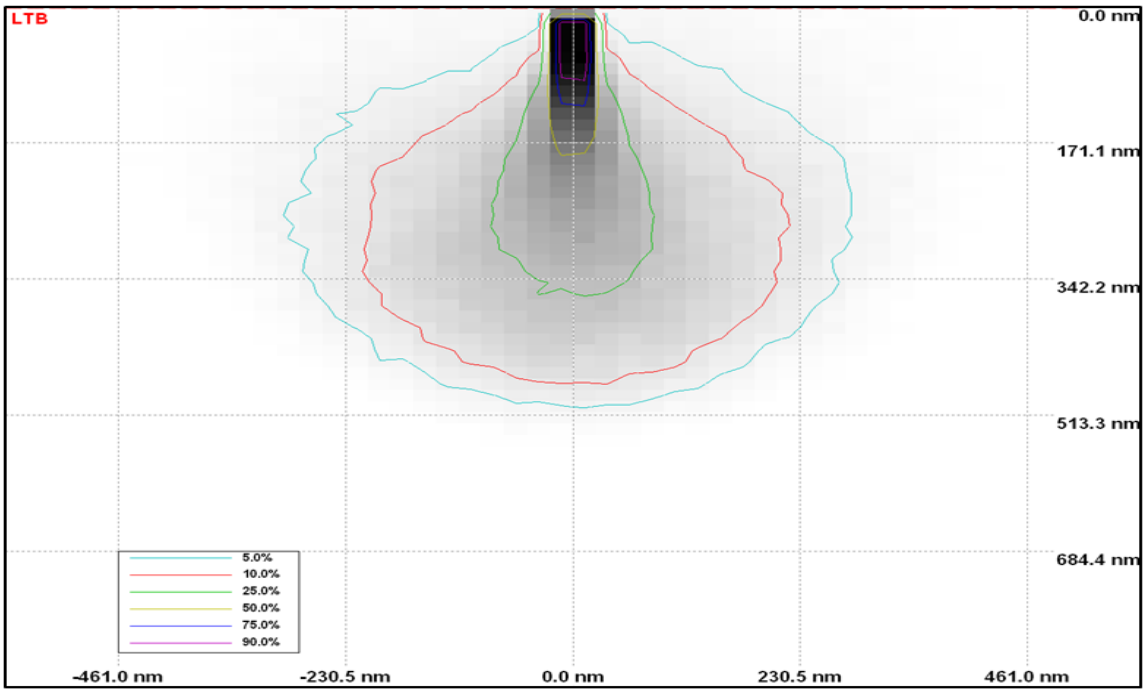

Figure 4-3: The energy retained by the incident primary electrons as a function of the radial displacement from the point of entry and depth into the material.

4.2 Cathodoluminescence Results

4.2.1 1st batch Ukrainian Undoped LTB

At first glance, the most obvious characteristic of this spectrum is the double-peak phenomenon that occurs in the 2.5-5 eV region at all temperatures, which can be seen in

Figure 4-4. Peaks in this region have been recorded in previous work and are universally attributed to self-trapped exciton emissions [6,27,28,13]. Interestingly, this region has generally been observed to be dominated by a single peak centered at 3.5 eV. However, this double peak was observed by Podgorska's experiment on a Manganese doped sample [21]. No explanation was offered for its presence, although it is assumed that it occurs from properties native to the LTB crystal and not from the Mn dopant.

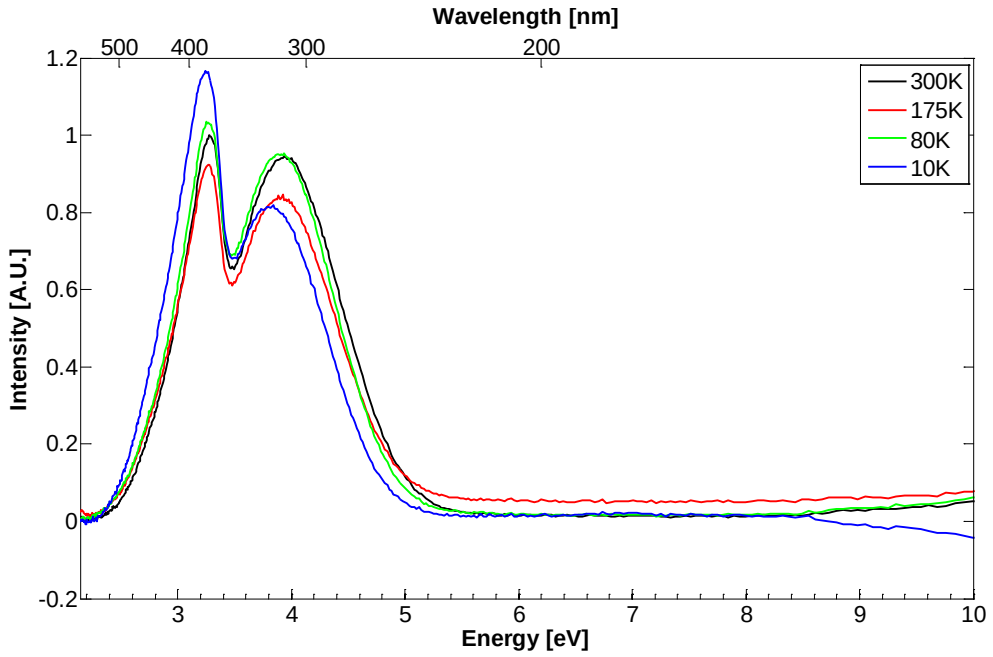

Figure 4-4: Cathodoluminescence spectrum of undoped LTB from the first Ukrainian-grown batch. A 5 keV electron energy with a 25 µA beam current was used. Different lines represent spectra taken at four different temperatures: (black) 300K, (blue) 10K, (green) 80K, and (red) 175 K.

Table 1: Wavelength and energy values of the peaks associated with the previous figure. Peak A is assigned to the high energy peak centered at 316-322 nm and Peak B is associated with the low energy peak at 378-381 nm.

10 K		
	λ [nm]	Energy [eV]
Peak A	322	3.85
Peak B	381	3.25

80 K		
	λ [nm]	Energy [eV]
Peak A	314	3.95
Peak B	380	3.26

175 K		
	λ [nm]	Energy [eV]
Peak A	316	3.92
Peak B	379	3.27

300 K		
	λ [nm]	Energy [eV]
Peak A	316	3.92
Peak B	378	3.28

From the results of this experiment, it is clear that the exciton emissions assigned to this region are composed of two strong fluorescent mechanisms. As temperature was varied from 10 K to room temperature, the relative intensity of the peaks changed as well. At 10 K, the relative intensity of Peak B is clearly lower than Peak A. However, at 300 K, the relative intensity of the two peaks is nearly equivalent. This trend is repeated with other samples. Furthermore, the energy (or wavelength) shift of the two peaks changed as well. Peak A shifts from 3.85 eV to 3.92 eV when raised from 10 K to 300 K, a difference of 0.13 eV. Peak B, on the other hand, shifts from 3.25 eV to 3.28 eV with the same temperature change, a difference of only 0.03 eV. This trend is also repeated with the other samples independent of doping. Peak A always underwent a greater wavelength shift with temperature than Peak B.

4.2.1.1 Theory of Behavior

This double peak can be explained as radiative annihilation of self-trapped excitons in the σ and π luminescence bands. Excitons may possess two different spin states (parallel or antiparallel) of the electron and hole components and can therefore

exist in the |1> (triplet) or |0> (singlet) spin states, corresponding to the π and σ luminescence bands respectively.

Since excitons are integer spin particles, they are subject to Bose-Einstein statistics in the low-density limit. Therefore, energy splitting between the singlet and triplet states can occur in otherwise identical particles. This behavior is represented in Figure 4-5.

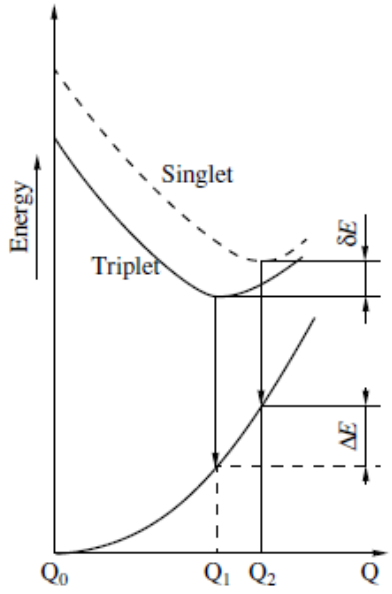

Figure 4-5: Adiabatic potential curve for the two lowest STE states in lithium tetraborate.

This figure shows the singlet state minimum having a configurational coordinate, Q_2, slightly larger than the triplet state minimum at Q_1. The energetic difference between the luminescence band maxima of the singlet and triplet states can be given by the equation

$$\Delta E_m = \delta E - \Delta E , \qquad (1.7)$$

which can be positive or negative depending on the numerical values. In LTB, ΔE_m has been previously determined to be –(300-400) meV, which means the triplet state should have a higher luminescence energy than the singlet state by 0.3-0.4 eV [29]. Based on

this argument, Peak A from this experiment corresponds to σ band luminescence from STE radiative annihilation while Peak B corresponds to the π band. The data from this experiment determines ΔE_m to be –(0.6-0.7) eV, which is in slight disagreement with this value.

The temperature dependence of the relative luminescence intensity between the two peaks occurs as a result of two mechanisms: the temperature dependence of the a^3N term and lithium ionic conductivity.

Tunneling recombination of an electron to a hole trapped on a defect site is a necessary step in STE production. Tunneling recombination kinetics is generally assumed to be temperature independent, although in some cases it is affected by temperature-dependent processes. The tunneling recombination kinetics term, a^3N, where a is the Bohr radius and N is the concentration of relevant defects, is proportional to the rate of electron tunneling to an excited state of a one-site small polaron to form STEs within the crystal. Essentially, it determines the rate at which STEs are produced and has positively correlated temperature dependence. The concentration of defects produced by an electron beam is generally considered to be temperature independent, which means the Bohr radius term drives the temperature dependence [28]. However, if electrons have a greater probability of tunneling to create STEs, it should increase the intensity of both peaks, not just Peak B. Therefore, this mechanism may explain a greater overall intensity in both peaks observed in Figure 4-7, but not the shift in relative intensity between the peaks.

The second temperature dependence of the luminescence bands occurs as a result of a diffusion-controlled annihilation of defects on the lithium sublattice. This will alter

the concentration of one of the tunneling pair components. At room temperature, lithium ions can migrate along the spontaneous-polarization direction of the crystal (the c axis) resulting in the annihilation of lithium interstitials and vacancies. This ionic current decreases with decreasing temperature, suppressing the rate of interstitial-vacancy annihilation. Furthermore, the theory of diffusion controlled reaction (DCR) predicts that this effect can only become manifest for events that occur on a comparatively long time scale [28]. Therefore, the fast decays of the singlet state electronic transitions means they will not be affected by this mechanism, whereas the long decay times for the triplet state transitions are. Therefore, Peak B should show a greater temperature dependence than Peak A which is, in fact, observed.

According to the figure, Peak B has a positive correlation of luminescence intensity to temperature. The ionic current essentially replaces lithium vacancies with Li^0 ions, altering the defect distribution throughout the crystal. Li^0 ions trap electrons that can be subsequently used in tunneling recombination to form a STE. The change in the defect distribution preferentially leads to the formation of spin |1> STEs, increasing the intensity of Peak B with respect to Peak A.

4.2.1.2 Alternate Theory

This double peak can be explained as emissions from inter-defect tunneling recombination of electrons to trapped holes to form self-trapped excitons in the vicinity of two different defect types that occur within the B-O complex of LTB. The tunneling recombination of electrons trapped on lithium sites to holes trapped on the anion complexes form small polarons in excited states. These polarons bind to the lattice near the defect they are trapped on forming self-trapped excitons in an excited state. The

excitons non-radiatively decay through phonon emission until they reach their ground state, where the carriers then recombine and emit a photon.

The typical anion complex in LTB consists of repeating B_4O_9 structures with two boron atoms in trigonal planar (written as Δ) oxygen environment (BO_3) and two boron atoms in the tetrahedral (written as □) environment (BO_4). The normal B-O complex is thus written as (2Δ+2□). However, due to the necessary overheating during the Czochralski growth technique to overcome the high melting points of the melt ingredients, oxygen vacancies proliferate. This results in defected B-O complexes in the form of three boron atoms in the trigonal planar oxygen configuration and one boron atom in the tetrahedral configuration (3Δ+1□), or it can create complexes with four boron atoms in the trigonal planar configuration (4Δ). Higher growth temperatures increase the ratio of Δ/□ creation in the crystal, generating these defects [13].

Self-trapped excitons must exist in the vicinity of defects or impurities in order to relax. As the exciton non-radiatively cascades down through its energy levels, it eventually reaches its ground state at E_n where n = 1, it subsequently radiatively decays through recombination of the electron and hole and simultaneous photon emission. The nature of the defect to which an STE is attached will perturb the binding energy of the STE, thus changing $E_{n=1}$. Since oxygen vacancies commonly occur in LTB, creating both (3Δ+1□) and (4Δ) complexes, each defective complex will change the value of E_n in its associated STEs, and hence adjust the wavelength of the emitted photon when the STE annihilates. This explains the observed two peaks in LTB in the vicinity of exciton annihilation energies.

The change in the relative peak height with temperature gives insight into which defective complex leads to which peak. The defective complexes are characterized by one oxygen vacancy in the case of (3Δ+1□) and two oxygen vacancies in the case of (4Δ). These create $(B_4O_8)^{-5}$ and $(B_4O_7)^{-4}$ complexes, respectively. The B-O complexes are known to trap holes since they are negatively charged point defects, which mean they trap the hole, or nuclei of the STE. The $(B_4O_8)^{-5}$ complex is a more efficient hole trap than the $(B_4O_7)^{-4}$ complex since it has more localized negative charge. At low temperatures, both complexes will be able to readily trap holes, and subsequently form STEs that annihilate, due to the low energy of the carriers. However, at higher temperatures, (3Δ+1□) complexes will trap holes more efficiently than the (4Δ), increasing the amount of STEs that decay near (3Δ+1□) complexes. This is observed as higher relative intensity of emissions decaying on the (3Δ+1□) complexes at higher temperatures. Therefore, it follows that Peak A is assigned to STE emissions that decay in the vicinity of the (3Δ+1□) B-O complexes, and Peak B is the same in vicinity of the (4Δ) complexes.

The previously observed 2.2 eV emission was not observed, even at liquid helium temperatures. However, due to the low response of the grating at the 564 nm wavelength region, this is not surprising.

4.2.2 2nd batch Ukrainian Undoped LTB

The cathodoluminescence results from the undoped LTB sample from the 2nd batch of Ukrainian grown crystals can be seen in Figure 4-7. The double peak is again seen and is similar to the undoped sample previously analyzed. The relative height of the peaks changes in the same way. Peak B grows in relative height to Peak A as

temperature is increased. However, the absolute intensity of the peaks decreases with temperature in a structured way. Both peaks clearly have a dependence on temperature, but the intensity of Peak B changes much more drastically than Peak A. Based on the previous explanation of the emissions, one would assume that emissions would increase with decreasing temperature since both complexes would become more efficient carrier traps. However, this is not observed. It can be explained by the lifetime of the STEs before they self trap. At higher temperatures, carriers have higher mobility, and will thus be able to move to a defect site quicker than at low temperatures. This reduces the lifetime of the STE before it self-traps and subsequently annihilates, resulting in increasing intensity of emissions at higher temperatures. This effect was mostly likely observed in this sample due to the higher crystal quality and the fact that fewer destructive experiments have been conducted on this particular sample. The absolute intensity of peaks between runs is usually of no consequence, but it follows a pattern and is of value in this particular case.

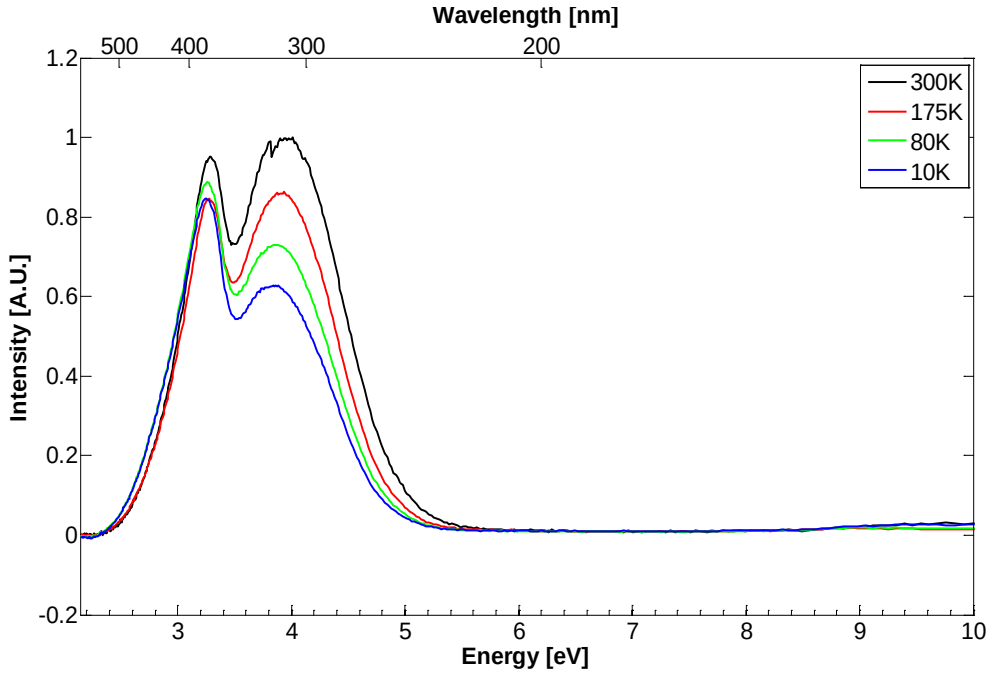

Figure 4-6: Cathodoluminescence spectrum of undoped LTB from the second Ukrainian-grown batch. A 5 keV electron energy with a 25 µA beam current was used. Different lines represent spectra taken at four different temperatures: (black) 300 K, (blue) 10 K, (green) 80 K, and (red) 175 K.

Table 2: Wavelength and energy values of the peaks associated with the previous figure. Peak A is assigned to the high energy peak centered at 311-320 nm and Peak B is associated with the low energy peak at 377-381 nm.

10 K		
	λ [nm]	Energy [eV]
Peak A	320	3.87
Peak B	381	3.25

80 K		
	λ [nm]	Energy [eV]
Peak A	320	3.87
Peak B	379	3.27

175 K		
	λ [nm]	Energy [eV]
Peak A	314	3.95
Peak B	377	3.29

300 K		
	λ [nm]	Energy [eV]
Peak A	311	3.98
Peak B	377	3.29

4.2.3 Newlight Undoped LTB

The cathodoluminescence results from the Newlight undoped LTB crystal sample can be seen in Figure 4-8. First, the behavior of Peak A and Peak B are consistent with

both Ukrainian doped samples. However, a very high energy peak at 7.60 eV was observed at low temperatures. It was not observed at room temperature and increased as temperature was decreased, reaching a maximum intensity at 10K, the lowest temperature achieved with this system. This inverse relation to temperature is an indicator that this emission is due to a deep donor or acceptor state. This can be explained in the following way. At high temperatures, deep donor and acceptor states will be filled with trapped carriers, but trapped carriers in shallow states can be easily thermally excited out of their traps and will have a short trapping lifetime. The crystal will preferentially decay to lower energy states through the unfilled shallow trapping states. However, at low temperatures, both shallow and deep trapping states will be filled and carriers will have a very low probability of being thermally excited from either. This increases the ratio of filled shallow states to filled deep states. With many of the shallow states unavailable as pathways to relax the crystal, the crystal begins to relax through deep donor and acceptor states. This explains the emission observed at Peak C.

Unfortunately, little is known about the growth technique of this particular crystal, so assigning this peak to any particular defect or impurity is not possible without further research or knowledge of the growth technique.

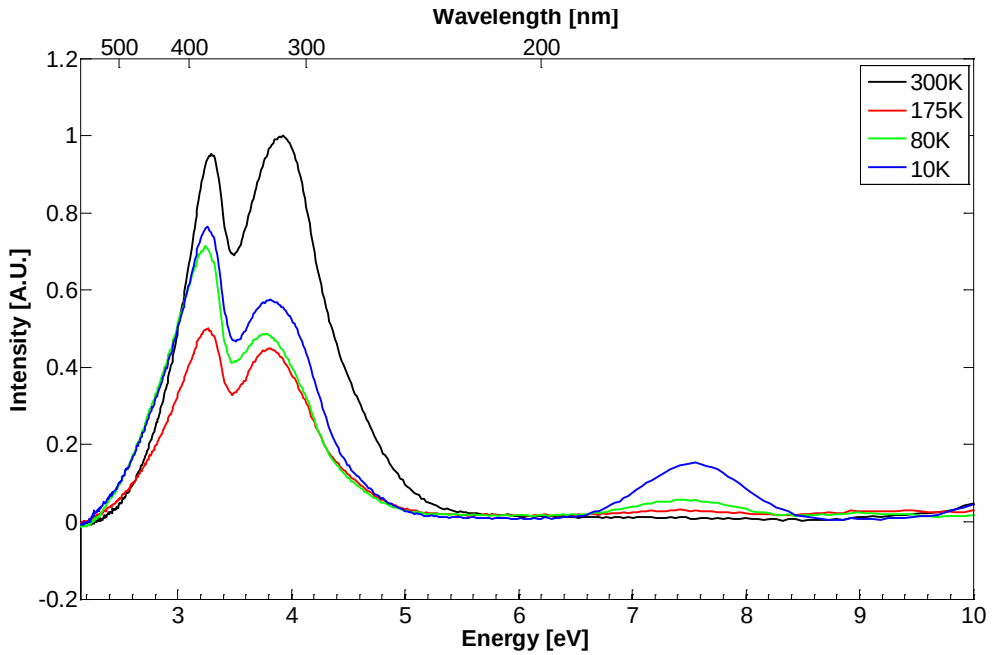

Figure 4-7: Cathodoluminescence spectrum of undoped LTB from Newlight, Inc.. A 5 keV electron energy with a 25 µA beam current was used. Different lines represent spectra taken at four different temperatures: (black) 300 K, (blue) 10 K, (green) 80 K, and (red) 175 K.

Table 3: Wavelength and energy values of the peaks associated with the previous figure. Peak A is assigned to the high energy peak centered at 315-328 nm and Peak B is associated with the low energy peak at 376-381 nm. Peak C, a unique peak associated with this sample, corresponds to the emissions observed at 161-163 nm.

10 K		
	λ [nm]	Energy [eV]
Peak A	325	3.81
Peak B	379	3.27
Peak C	163	7.60

80 K		
	λ [nm]	Energy [eV]
Peak A	328	3.78
Peak B	381	3.25
Peak C	161	7.70

175 K		
	λ [nm]	Energy [eV]
Peak A	326	3.80
Peak B	381	3.25
Peak C	163	7.60

300 K		
	λ [nm]	Energy [eV]
Peak A	315	3.93
Peak B	376	3.30

4.2.4 LTB: Ag

The cathodoluminescence results from the LTB: Ag crystal sample can be seen in Figure 4-9. The addition of the Ag doping significantly alters the CL spectrum. Silver is a known activator and the Ag^{+1} ion has a metal-centric $4d^9 5s \rightarrow 4d^{10}$ electronic transition that emits at ~ 4.62 eV, nearly exactly where this peak is observed in this experiment. It is thus logical to assign Peak C to this mechanism. This peak is so intense at room temperature that it masks the exciton peaks observed in the undoped LTB temperatures. However, it has a strong temperature dependence and loses most of its intensity at very low temperatures, allowing the exciton peaks to be observed. Peak A, the high energy exciton peak is only observed at 10K, although is most likely present at the other temperatures. However, its location is similar to the undoped samples. The same is true for Peak B, which can be clearly seen in the inset graph of Figure 4-9. It also behaves similarly to the undoped crystalline samples.

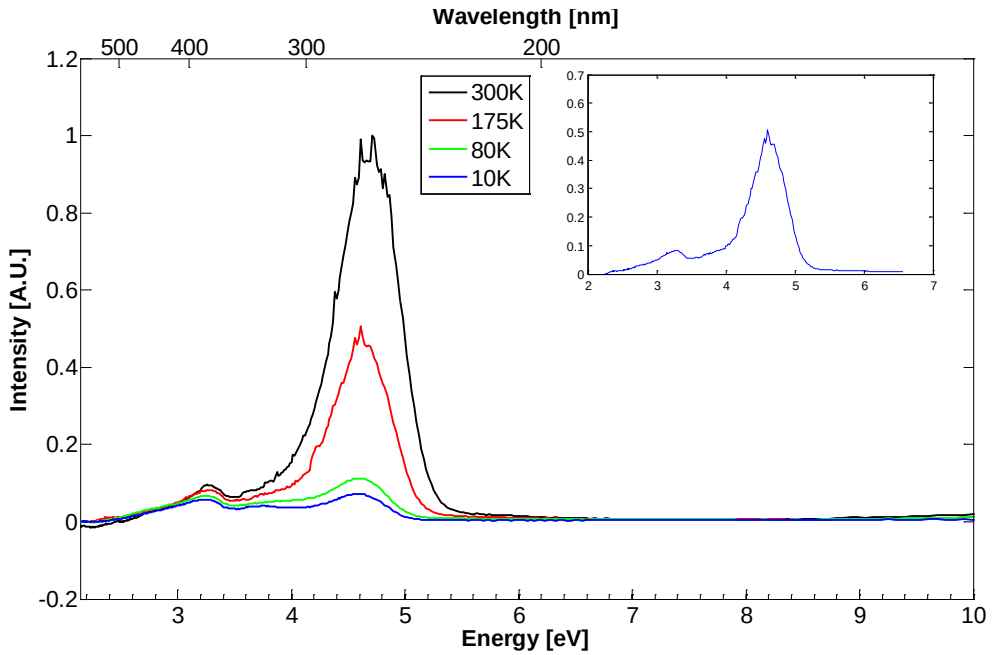

Figure 4-8: Cathodoluminescence spectrum of Ukrainian-grown LTB: Ag. A 5 keV electron energy with a 25 µA beam current was used. Different lines represent spectra taken at four different temperatures: (black) 300 K, (blue) 10 K, (green) 80 K, and (red) 175 K. In the inset is a magnified view of the 10 K data since the shape of the curve is lost on the normal intensity scale.

Table 4: Wavelength and energy values of the peaks associated with the previous figure. Peak A is assigned to the high energy peak centered at 329 nm and Peak B is associated with the low energy peak at 378-382 nm. Peak C, a unique peak associated with this sample assigned to a silver activator electronic transition, corresponds to the emissions observed at 263-271 nm.

10 K

	λ [nm]	Energy [eV]
Peak A	329	3.77
Peak B	382	3.24
Peak C	271	4.57

80 K

	λ [nm]	Energy [eV]
Peak B	378	3.28
Peak C	270	4.59

175 K

	λ [nm]	Energy [eV]
Peak B	380	3.26
Peak C	268	4.62

300 K

	λ [nm]	Energy [eV]
Peak B	378	3.28
Peak C	263	4.71

4.2.5 LTB: Cu

The cathodoluminescence results from the LTB: Cu crystal sample can be seen in Figure 4-10. The copper doping significantly altered the CL spectrum from an undoped sample. Though no new peaks are observed, Peak B demonstrates a much higher relative intensity than Peak A, even at room temperature where Peak A dominated in the undoped samples. This is explained by the energy scheme of the Cu^{+1} ion, which substitutes in the Li^{+1} location within the crystal. Cu^{+1} has a $3d^9 4s \rightarrow 3d^{10}$ metal-centered electronic transition that covers the energy range 2.7-3.3 eV. At this energy level, it will create an energy peak that is superimposed onto the excitonic emission at Peak B, increasing its apparent intensity with respect to the higher energy Peak A. Assuming the activator intensity is strongly, yet inversely dependent on temperature as it was in the silver doped sample, one would expect the relative intensity of Peak B to drop at low temperatures. This is, in fact, observed with the spectrum obtained at 80K, although it seems to recover somewhat at 10K.

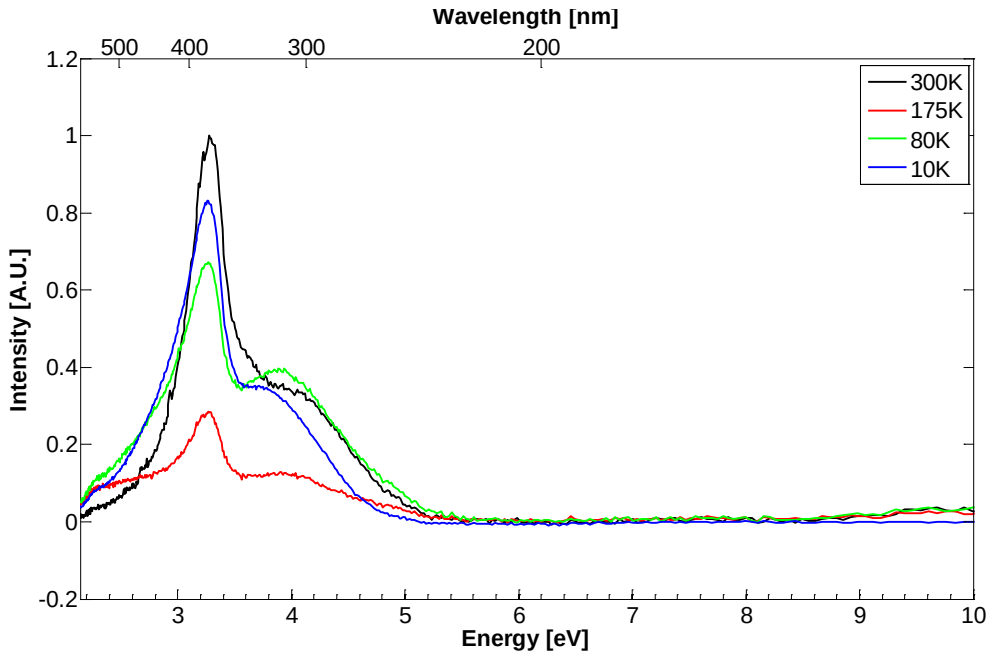

Figure 4-9: Cathodoluminescence spectrum of Ukrainian-grown LTB: Cu. A 5 keV electron energy with a 25 µA beam current was used. Different lines represent spectra taken at four different temperatures: (black) 300 K, (blue) 10 K, (green) 80 K, and (red) 175 K.

Table 5: Wavelength and energy values of the peaks associated with the previous figure. Peak A is assigned to the high energy peak centered at 305-331 nm and Peak B is associated with the low energy peak at 378-381 nm.

10 K		
	λ [nm]	Energy [eV]
Peak A	331	3.74
Peak B	379	3.27

80 K		
	λ [nm]	Energy [eV]
Peak A	314	3.95
Peak B	381	3.25

175 K		
	λ [nm]	Energy [eV]
Peak A	317	3.91
Peak B	379	3.27

300 K		
	λ [nm]	Energy [eV]
Peak A	305	4.06
Peak B	378	3.28

4.2.6 LTB: Mn

The cathodoluminescence results from the LTB: Mn crystal sample can be seen in Figure 4-10. The relative intensities of Peak A and Peak B demonstrate the same patterns as they do in the undoped samples. A minimal intensity, low energy peak was observed at ~ 2 eV at room temperature, but was not observed at lower temperatures. This may be an indicator of green band luminescence observed in other luminescence experiments with Mn doped LTB [21]. However, the spectral response of the grating used in this experiment is very poor at these wavelengths and may not indicative of crystal emissions. However, this would explain why this was the only sample to appear to glow green under irradiation instead of blue as all the other samples.

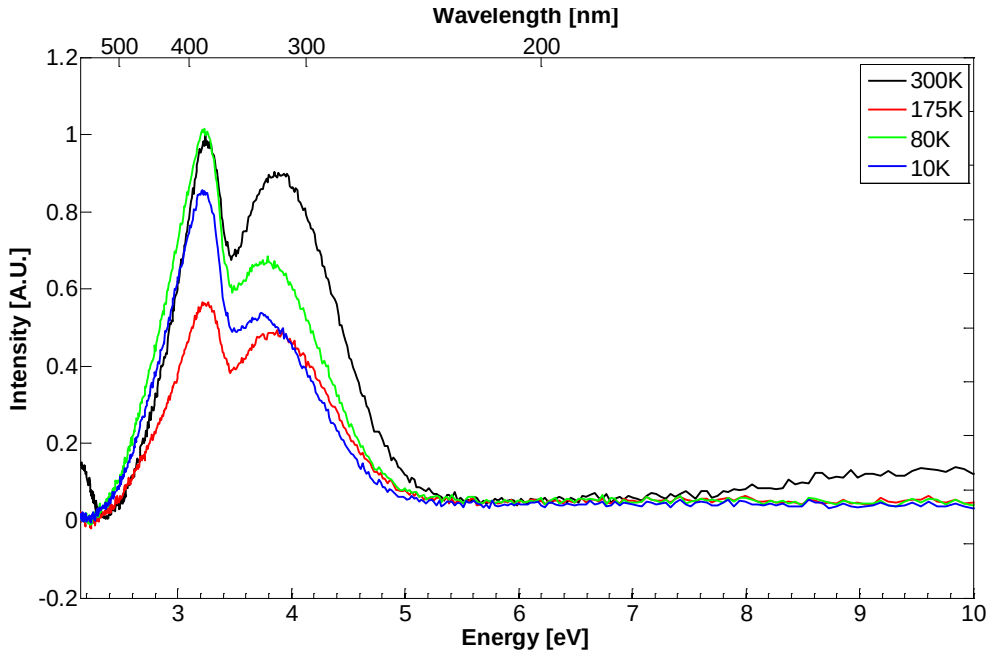

Figure 4-10: Cathodoluminescence spectrum of Ukrainian-grown LTB: Mn. A 5 keV electron energy with a 25 µA beam current was used. Different lines represent spectra taken at four different temperatures: (black) 300 K, (blue) 10 K, (green) 80 K, and (red) 175 K.

Table 6: Wavelength and energy values of the peaks associated with the previous figure. Peak A is assigned to the high energy peak centered at 319-331 nm and Peak B is associated with the low energy peak at 382-386 nm.

10 K		
	λ [nm]	Energy [eV]
Peak A	331	3.74
Peak B	386	3.21

80 K		
	λ [nm]	Energy [eV]
Peak A	326	3.80
Peak B	383	3.23

175 K		
	λ [nm]	Energy [eV]
Peak A	319	3.88
Peak B	383	3.23

300 K		
	λ [nm]	Energy [eV]
Peak A	319	3.88
Peak B	382	3.24

4.3 Thermoluminescence Results

The results for the TL data for the LTB: Cu sample can be seen in Figure 4-12. The bimodal nature of the emission is consistent with Hunda et al [14]. However, temperature values for the peaks are slightly shifted in the higher temperature direction in this experiment. This can be attributed to the difference in heating rates. This experiment used a 1˚C/s heating rate, whereas 2.90˚C/s was previously used. Hunda et al. most likely missed the true value of the emission temperature due to their faster

heating rate.

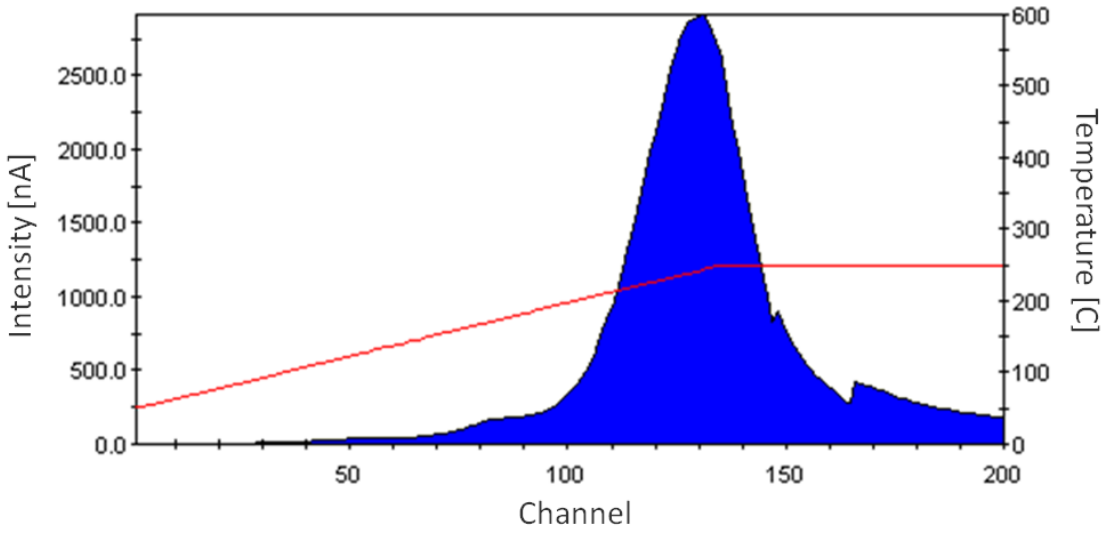

Figure 4-11: TL results of the LTB: Cu sample after electron irradiation. Peaks can be seen at 178˚C and 250˚C.

Furthermore, relative peak intensities are shifted as well. In this experiment the intensity of the high temperature peak is much larger compared with the intensity of the low temperature peak than in Hunda's results. There are two possible explanations for this. First, the crystal used in this experiment could simply possess a higher relative concentration of defects associated with the high temperature peak. The crystal would then trap more carriers at that energy level, and fluoresce with higher intensity when the temperature is raised. The alternative explanation is that the nature of the ionizing radiation changed the fill probabilities of these two different trapping levels. The electron radiation may have set the conditions for a higher tendency for free carriers to occupy the trap associated with the high temperature peak.

The results of the TL data for the LTB: Ag sample can be seen in Figure 4-13. The behavior of the crystal is similar to Brant et al [9]. A single peak exists, indicating that

the electron trap and hole trap thermally destabilize in a close temperature range. However, the temperature at which this happens is slightly different. With a heating rate of 1˚C/s, the peak in this experiment is observed at 196˚C. Brant encountered this same peak in the range of 160˚C to 177˚C depending on heating rate. The most likely reason for this inconsistency is the high uncertainty of the Harshaw TLD reader in comparison to the more sophisticated Riso TL/OSL reader that Brant used at the University of Cincinnati [9].

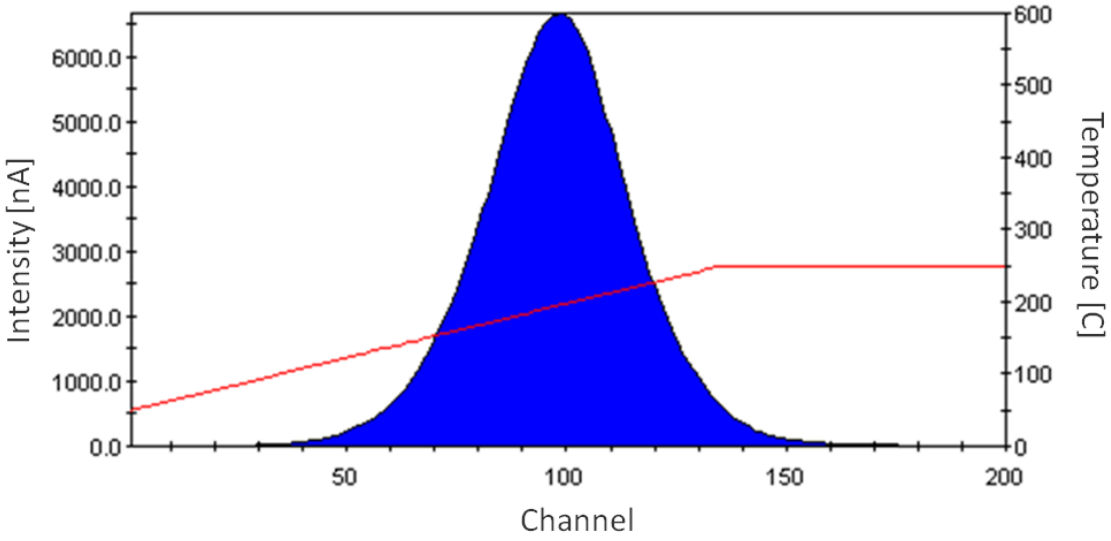

Figure 4-12: TL data for LTB: Ag irradiated with 5 keV electrons. A single peak at 196˚C is observed.

The results of the TL experiment on the LTB: Mn sample can be seen in Figure 4-14. According to Lorrain et al., LTB: Mn demonstrates a bimodal TL behavior with peaks centered on 100˚C and 235˚C [30]. In this experiment, only one peak at 225˚C is observed. This is mostly likely the same peak as the 235˚C peak in Lorrain's paper, while the 100˚C peak was not observed. Furthermore, note that the intensity of the emission is much lower than the LTB: Ag, Cu samples. This is due to the fact that

manganese is only commonly found in the +2 oxidation state. With the inability to form an A^0 center, or even an A^{+1} center, the electron trapping ability of the Mn ion is reduced compared to the copper or silver. As the holes are thermally destabilized into free carriers, they find fewer electrons trapped by the Mn ions with which to form excitons and radiatively decay.

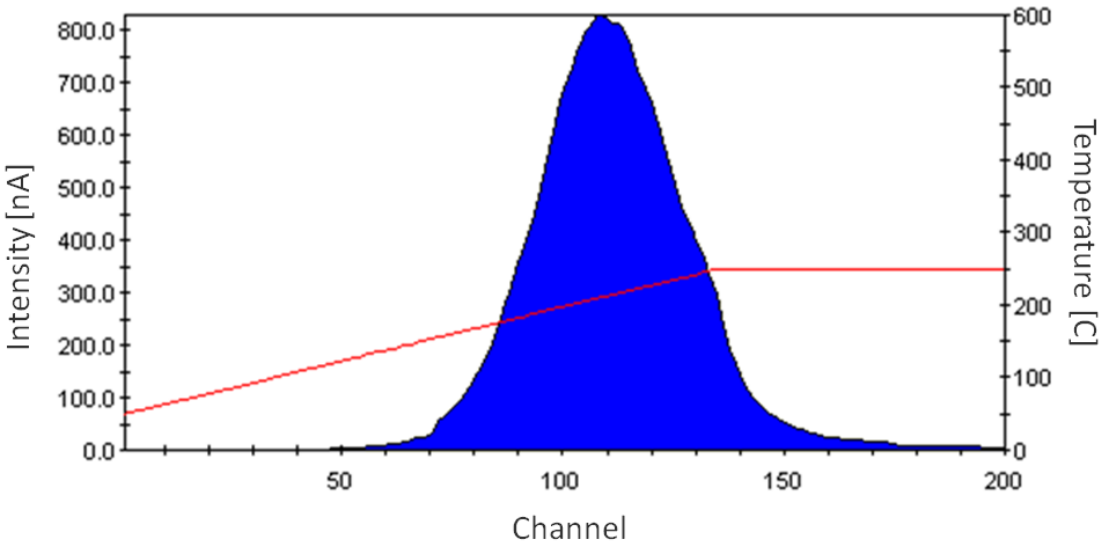

Figure 4-13: TL data for the LTB: Mn sample after irradiation with 5 keV electrons. A single peak at 225˚C is observed.

For the three undoped samples, the results for the 1st generation Ukrainian grown undoped sample can be seen in Figure 4-15, the 2nd generation undoped Ukrainian grown sample can be seen in Figure 4-16, and the Newlight undoped sample can be seen in Figure 4-17. All three samples demonstrate bimodal behavior in their glow curves with peak 1 centered between 165 and 198˚C and the second peak near 250˚C. Recall the TLD reader only heated to 250˚C with a short anneal at this temperature. The low temperature peak shifted quite significantly, indicating a different environment for this

carrier trap from crystal to crystal. Furthermore, the relative heights of the peaks changed quite significantly as well, indicating the density of the traps also changed.

Overall the luminescent intensity for the undoped crystals was much lower than the doped samples. This is due to the fact that lithium only commonly occurs in the +1 oxidation state. Unlike silver and copper, lithium cannot form an A^0 center, thus making it a much less efficient electron trap, reducing the available sites at which free holes can form an exciton. The result of drastically reduced charge trapping ability is the reduction of luminescence upon heating, which is observed in all the undoped samples, particularly the Newlight sample, which has a maximum intensity of just 1.4 nA.

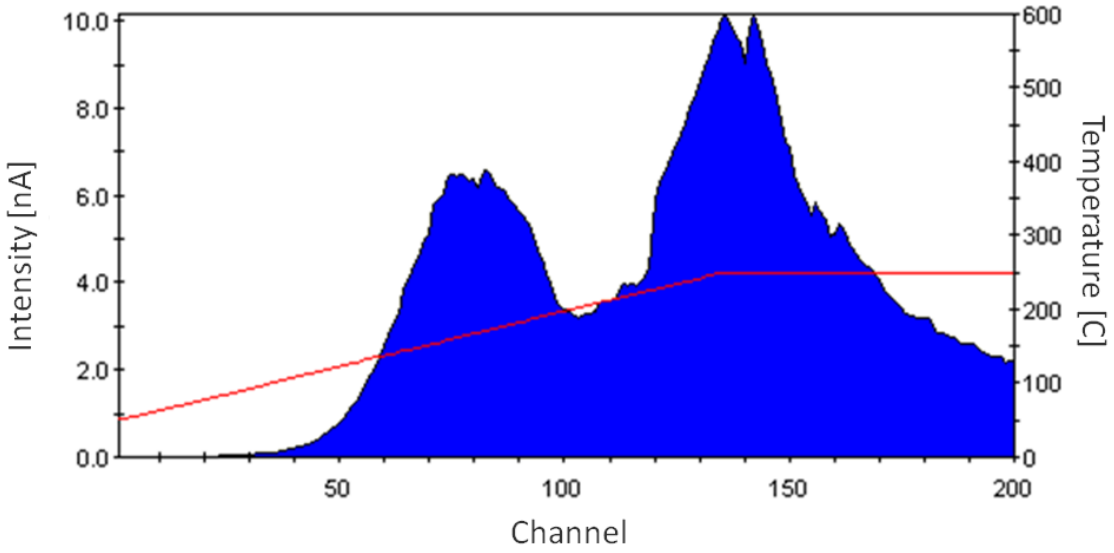

Figure 4-14: TL data for the undoped LTB sample from the first batch of Ukrainian grown samples. Peaks are observed at 165˚C and 250˚C.

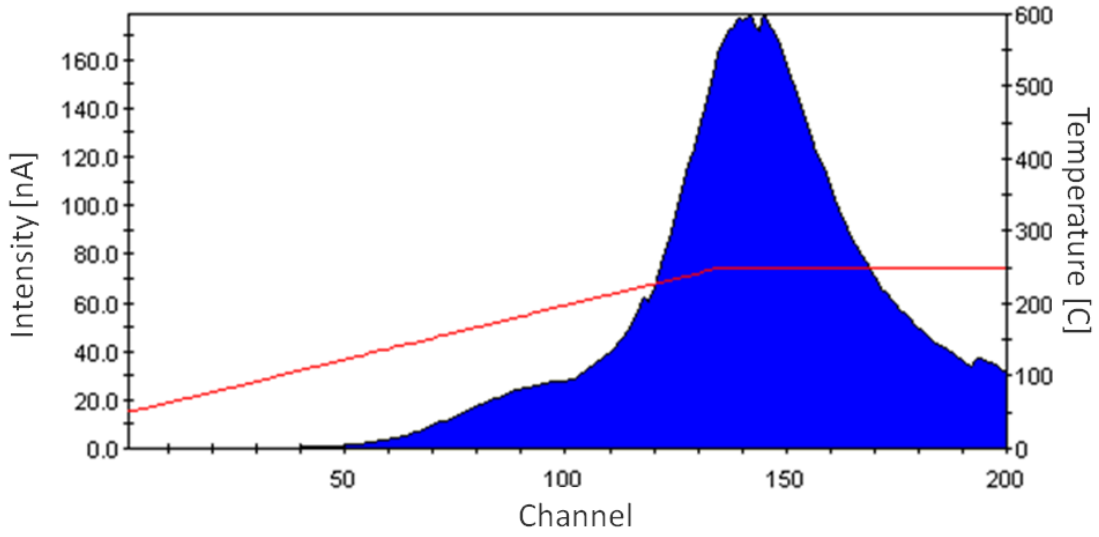

Figure 4-15: TL data for the undoped LTB sample from the second batch of Ukrainian grown samples. Peaks are observed at 195˚C and 250˚C.

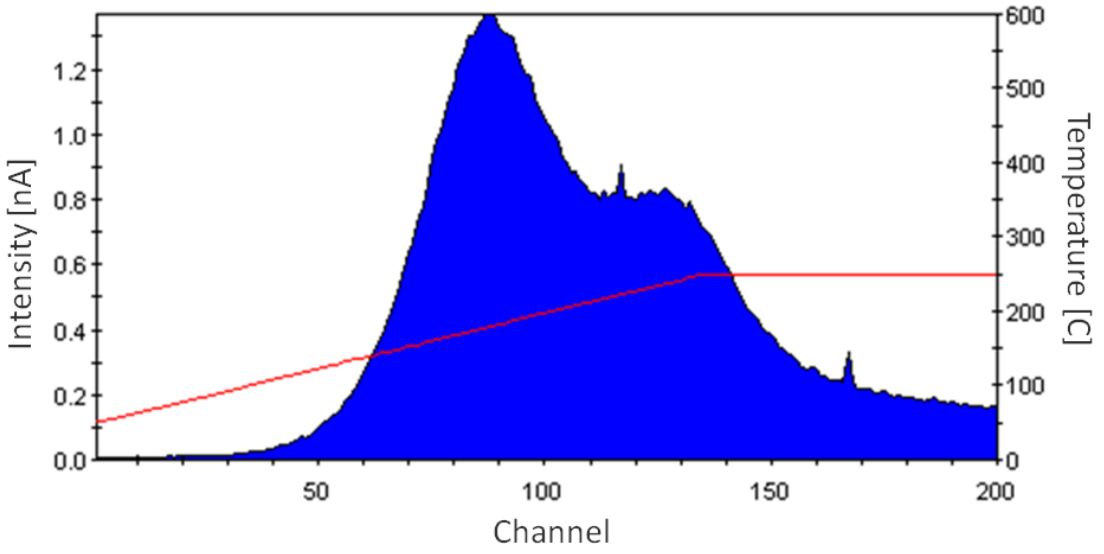

Figure 4-16: TL data from the undoped LTB sample grown by Newlight. Peaks are observed at 178˚C and 245˚C.

V. Conclusion

In this chapter, the development of the experiment and its results will be briefly summarized. Some additional comments will be made regarding avenues of future research.

5.1 Summary of Results

5.1.1 Cathodoluminescence

The results of this experiment showed that the exciton emission region from LTB in the 2.5-5.0 eV energy range is actually comprised of two distinct peaks. Based on the behavior of these peaks as a function of temperature, the two peaks are assigned to STE emissions from two different spin states of the exciton. The lower energy peak, around 3.25 eV, occurs as a result of STE emission from the σ, or |0> spin state while the higher energy peak, around 3.90 eV is from emissions of STEs in the π or |1> spin state. E_m, the energy difference between the maxima of the two peaks was calculated at –(0.5-0.9) eV, slightly more negative than a previously reported value [28].

Doping the samples produced peaks in previously known areas. The Ag^{+1} ion demonstrated its characteristic metal-centric $4d^9 5s \rightarrow 4d^{10}$ electronic transition that emits at 4.62 eV. Similarly, the Cu^{+1} ion demonstrated its $3d^9 4s \rightarrow 3d^{10}$ metal-centered electronic transition that covers the energy range 2.7-3.3 eV. Observing these materials with the VUV system at previously untested high energy ranges and at extremely low temperatures did not reveal any additional emissions. It did, however, characterize the behavior of the known phenomena at very low temperatures. The LTB: Mn crystal did not change the spectra from what the undoped samples produced. Due to the increase of

luminescence intensity, Ag doped LTB is the best candidate to pursue research for a scintillating detector.

5.1.2 Thermoluminescence

The results of this experiment showed that lithium tetraborate behaved similarly after electron irradiation as it did under x-ray irradiation from previous experiments. The double peaked nature of the copper doped sample was very similar to previous results, while the single silver doped sample was as well. Undoped samples all showed similar behavior with a bimodal distribution in the range tested. The manganese doped samples were the only ones that did not behave similarly to previous research. Previous work observed a 100℃ emission that was not observed in this experiment. Based on the increase in luminescence intensity, Ag doped LTB would make the best candidate for a TLD type detector.

5.2 Future Research

Several experiments come to mind to follow this research. The first and most relevant is to reproduce this research with different experimental techniques. For example, one could use different methods of sample preparation to mitigate the effects of surface charging. Evaporating a very thin layer of conducting material such as gold over the surface of the material may serve to significantly minimize photovoltaic charging. A shift in the peaks may indicate the previous influence of charging on the radiative spectrum.

A depth-resolved dependence on the cathodoluminescent spectrum could provide insight in the to the surface state formation as one approaches the surface of the crystal. According to CASINO calculations, one would need an electron energy of close to 1 keV

to deposit a significant portion of the energy within 50 nm of the surface. The problem is that when using such a low energy, fewer free carriers are created, reducing the radiative signal. One would need to use an electron source that could produce a much larger beam current than the one used in this experiment in order to sufficiently excite the target material. This would mostly likely include the purchase of a new low-energy, high-current electron gun to use in the lab.

Timing information would be invaluable in interpreting the cause behind several of the observed peaks in the radiative spectrum of LTB and other materials. This can be achieved through the use of a pulsed electron source and equipment designed to detect time-dependent photon emission. The SR430 used in this experiment is the perfect tool for the latter. It uses bins to detect pulses and extract the timing information. It also has the ability to synchronize TTL pulses to initiate the electron pulse and begin recording photon emissions from the source. The Kimball Physics EMG-14 and EMG-12 come with a beam blanking option that can be used to pulse the electron beam. It does this by generating a cyclic potential that rasters the beam on and off the source. Unfortunately, it generates a pulse width of ~ 1 μs. This is sufficient to interpret some longer decay pathways, but not nearly small enough to resolve very fast radiative decay mechanisms in a sample. One can purchase an upgrade to the electron gun that generates a grid pulsing option that reduces the pulse width to 50 ns. With this upgrade, one can extract relatively fast signals with the SR430. With a minimum bin width of 5 ns, only the first few bins would be skewed with the 50 ns pulse.

Another experiment is to conduct CL on the eight rare-earth doped samples of LTB. Rare earth elements, when dopants, are known intense activators that generally

fluoresce in the visible region. The lab has a CL system designed to be used in the visible region, although some samples may emit in the ultraviolet region as well. The location of these activator levels in LTB could prove valuable in the future fabrication of a device.

The goal of Department of Defense research into lithium tetraborate is to eventually create a solid state neutron detection material. Based on this work and previous work on the material, a scintillating device would be a viable option to pursue. An experiment similar to this research, but using neutrons as the exciting source could be the next step in the process. Neutrons will ionize atoms in the material through knock on damage and nuclear reactions of the lithium and boron atoms within the material. As the neutrons elastically collide with nuclei in the target material, the displaced atoms will ionize other atoms as it moves through the material. Similarly, since LTB is rich in both Li and B, both with isotopes with large neutron capture cross sections, fissioned Li and B nuclei can also ionize other atoms as they proceed through the crystal. This ionization creates free carriers similar to the incident electrons from this experiment, although they do create more damage in the process. Regardless, the free carriers will seek lower energy configurations via the same pathways as in cathodoluminescence, creating a photon signal able to be detected. If one were to use a spectrometer with a CCD as opposed the monochromator used in this experiment, one could extract the instantaneous luminescent spectrum from a sample excited by neutrons. Since the spectrum that LTB radiates in is now known, one could calibrate the spectrometer to be responsive in those wavelength regions.

The thermoluminescence done in this experiment was conducted using the Harshaw TLD reader in building 470. This equipment comes with some significant constraints that compromise the scientific validity of the results. First of all, it is limited to a 1°C per second heating rate. Slower heating rates are needed to reduce the error in the experiment. Second, it does not allow the data to be extracted from the software once the experiment is completed. One is left to only qualitatively looking at the plots instead of looking at the data and determining where events occur. Using electrons as the source of ionizing radiation, a better device could be used to conduct another thermoluminescence experiment that was better suited to control and extract data for scientific purposes and at a broader range of temperatures.

As a modeling project, one could attempt to model the thermoluminescence kinetics of the lithium tetraborate crystals. Dr. I.N. Ogorodnikov of the Ural Federal University in Ekaterinburg, Russia wrote a paper outlining the general method he used to create such a model. It uses a system of differential equations of balance that follow:

$$\begin{aligned}
&\frac{dn_i}{dt} = (P_{ex}h_i + A_i N^-)\cdot(\nu_i - n_i) - \omega_i n_i;\\
&\frac{dn_k}{dt} = (P_{ex}h_k + A_k N^+)\cdot(\nu_k - n_k) - \omega_k n_k;\\
&\frac{dN^-}{dt} = P_{ex} + \sum_i(\omega_i n_i - A_i N^-(\nu_i - n_i)) + \sum_k (P_{ex}h_k(\nu_k - n_k) - r_k n_k N^-);\\
&\frac{dN^+}{dt} = P_{ex} + \sum_k(\omega_k n_k - A_k N^+(\nu_k - n_k)) + \sum_i (P_{ex}h_i(\nu_i - n_i) - r_i n_i N^+);\\
&0 = N^- + \sum_i n_i - N^+ - \sum_k n_k.
\end{aligned} \tag{1.8}$$

P_{ex} is the rate of transitions of electrons from the valence band to the conduction band under excitation, N^- is the concentration of electrons in the conduction band, N^+ is the concentration of holes in the valence band, h_k and h_i are factors that describe potential

traps getting filled by the transitions, A_k and A_i are trapping rates for the holes and electrons, v_k and v_i are the concentrations of available centers for trapping holes and electrons, n_k and n_i are concentrations of holes and electrons trapped on the centers, r_k and r_i are the recombination rates of the trapped hole and electron centers, k and i are indices denoting hole and electron centers, and ω_k and ω_i represent probabilities of thermally stimulating delocalization of holes and electrons. These probabilities are based on the Maxwell-Boltzmann distribution of particles at any input temperature [31]. A model of this nature along with precision thermoluminescence data on LTB would be invaluable to understanding the properties of this material.

VI. Bibliography

[1] Ya.V. Burak, B.V. Padlyak, and V.M. Shevel. "Radiation-induced centers in the Li2B4O7 single crystals." *Nuclear Instruments and Methods in Physics Research Section B: Beam Interactions with Materials and Atoms,* 191, Issues 1–4 (May 2002): 633-637.

[2] B. E. Kananen. "Characterization of neutron-induced defects in isotopically enriched lithium tetraborate." MS Thesis, Air Force Institute of Technology, 2011.

[3] M. W. Swinney, J. W. McClory, J. C. Petrosky, Shan Yang, A. T. Brant, V. T. Adamiv, Ya. V. Burak, P. A. Dowben, and L. E. Halliburton. "Identification of electron and hole traps in lithium tetraborate ($Li_2B_4O_7$) crystals: Oxygen vacancies and lithium vacancies." *Journal of Applied Physics* 107, 113715 (2010).

[4] V.T. Adamiv, Ya.V. Burak, and I.M. Teslyuk. "The crystal structure of $Li_2B_4O_7$ compound in the temperature range 10–290 K." *Journal of Alloys and Compounds,* 475 (2009): 869-873.

[5] C. L. Dugan. "Cathodoluminescence and photoemission of doped lithium tetraborate." MS Thesis, Air Force Institute of Technology, 2011.

[6] V.T.Adamiv, V.P.Savchyn, P.V.Savchyn, I.M.Teslyuk, and Ya.V.Burak. "Influence of isovalent doping on the cathodoluminescence of $Li_2B_4O_7$:A (A = K, Cu, Ag) single crystals." *Functional Materials,* 16, no. 3 (2009): 247-252.

[7] D. J. Wooten. "Electronic structure of lithium tetraborate." PhD dissertation, Air Force Institute of Technology, 2010.

[8] J. G. Gualtieri, J. A. Kosinski, W. D. Wilber, Y. Lu, S. T. Lin, M. Murray, and W. Ruderman. "Dilithium tetraborate ($Li_2B_4O_7$) fabrication technology." *Proceedings of the 46th IEEE Frequency Control Symposium* (1992): 724-731.

[9] A. T. Brant, B. E. Kananan, M. K. Murari, J. W. McClory, J. C. Petrosky, V. T. Adamiv, Ya. V. Burak, P. A. Dowben, and L. E. Halliburton. "Electron and hole traps in Ag-doped lithium tetraborate ($Li_2B_4O_7$) crystals." *Journal of Applied Physics* 110, 093719 (2011).

[10] V.T. Adamiv, Ya.V. Burak, I.V. Kityk, J. Kasperczyk, R. Smok, and M. Czerwiński. "Nonlinear optical properties of $Li_2B_4O_7$ single crystals doped with potassium and silver." *Optical Materials* 8, no. 3 (1997): 207-213.

[11] M. M. Islam, V. V. Maslyuk, T. Bredow, and C. Minot. "Structural and electronic properties of $Li_2B_4O_7$." *Journal of Physical Chemistry B* 109, no. 28, 13597 (2005).

[12] J. T. Randall and M. H. F. Wilkins. "Phosphorescence and Electron Traps. I. The Study of Trap Distributions." *Proceedings of the Royal Society of London A* 184, no. 999 (1945): 365-389.

[13] V. T. Adamiv, O. T. Antonyak, Ya. V. Burak, M. S. Pidzyrailo, and I. M. Teslyuk. "Model of TSL-centers in $Li_2B_4O_7$:A (A = Cu, Ag) single crystals." *Functional Materials* 12, no. 2 (2005): 278-281.

[14] B. M. Hunda, T. V. Hunda, P. P. Puga, A. M. Solomon, V. M. Holovey, and G. D. Puga. "Concentration and Temperature Dependence of Luminescence for the Copper-Doped Lithium Tetraborate Single Crystals." *Journal of Optoelectronics and Advanced Materials* 1, no. 4 (1999): 49–56.

[15] A. Holmes-Siedle and L. Adams. *Handbook of Radiation Effects*, 2 ed.. New York NY: Oxford University Press, 2002.

[16] D. R. Vij. *Luminescence of Solids.* New York NY: Plenum Press, 1998.

[17] P. R. Thornton. *The Physics of Electroluminescent Devices.* London UK: E. & F. N. Spon, 1967.

[18] B. G. Yacobi and D. B. Holt. *Cathodoluminescence Microscopy of Inorganic Solids.* New York, NY: Springer, 1990.

[19] N. F. Mott and A. M. Stoneham. "The lifetime of electrons, holes and excitons before self-trapping." *Journal of Physics C: Solid State Physics* 10, no. 17 (1977) 3391-3398.

[20] M. Ignatovych, V. Holovey, T. Vidóczy, P. Baranyai, and A. Kelemen. "Spectral study on manganese- and silver-doped lithium tetraborate phosphors." *Radiation Physics and Chemistry* 76 (2007): 1527-1530.

[21] D. Podgórska, S.M. Kaczmarek, W. Drozdowski, M. Berkowski, and A. Worsztynowicz. "Growth and Optical Properties of $Li_2B_4O_7$ Single Crystals Pure and Doped with Yb, Co and Mn Ions for Nonlinear Applications." *Acta Physica Polonica A* 107, no. 3 (2005): 507-518.

[22] Kimball Physics, Inc.. *Operator's Manual: EMG-14/EGPS-14 Electron Gun and Power Supply*. Wilton NH: Kimball Physics, Inc., 1999.

[23] McPherson, Inc.. *Operator's Manual: Model 234/302 UHV Monochromator*. Chelmsford MA: McPherson, Inc..

[24] Hamamatsu Photonics K. K.. *Operator's Manual: Hamamatsu Photomultiplier Tubes R6094, R6095*. Shizuoka-ken Japan: Hamamatsu Photonics K. K., 1996.

[25] Stanford Research Systems. *Operator's Manual: Multichannel Scaler/Averager Model SR430*. Sunnyvale CA: Stanford Research Systems, 1999.

[26] Saint-Gobain Crystals & Detectors. *Operator's Manual: Model 3500 Manual TLD Reader with WinREMS*. Solon OH: Saint-Gobain Crystals & Detectors, 2001.

[27] V. T. Adamiv, Ya. V. Burak, D. J. Wooten, J. McClory, J. Petrosky, I. Ketsman, J. Xiao, Y. B. Losovyj, and P. A. Dowben. "The Electronic Structure and Secondary Pyroelectric Properties of Lithium Tetraborate." *Materials* 3, no. 9 (2010): 4550-4579.

[28] I. N. Ogorodnikov, V. Yu. Yakovlev, A. V. Kruzhalov, and L. I. Isaenko. "Transient optical absorption and luminescence in $Li_2B_4O_7$ lithium tetraborate." *Physics of the Solid State* 44, no. 6 (2002): 1039-1047.

[29] I. N. Ogorodnikov, V. A. Pustovarov, A. V. Kruzhalov, L. I. Isaenko, M. Kirm, and G. Zimmerer. "Self-trapped excitons in LiB_3O_5 and $Li_2B_4O_7$ lithium borates: Time-resolved low-temperature luminescence VUV spectroscopy." *Physics of the Solid State* 42, no. 3 (2000): 464-472.

[30] S. Lorrain, J. P. David, R. Visocekas, and G. Marinello. "A Study of New Preparations of Radiothermoluminescent Lithium Borates with Various Activators." *Radiation Protection Dosimetry* 17, no 1-4 (1986): 385-392.

[31] I.N. Ogorodnikov and N.E. Poryvai. "Thermoluminescence kinetics of lithium borate crystals." *Journal of Luminescence* 132, no. 6 (2012): 1318-1324.

[32] W. E. Spicer. "Luminescence from Sodium Chloride." *Physical Review* 106, no. 4 (1957): 726-732.

[33] J. L. McFall. *Optical Investigation of Molecular Beam Epitaxy Al_xGa_1-xN to Determine Material Quality*. MS Thesis, Air Force Institute of Technology, 2000.

VII. Appendix A: Supplementary CASINO Data

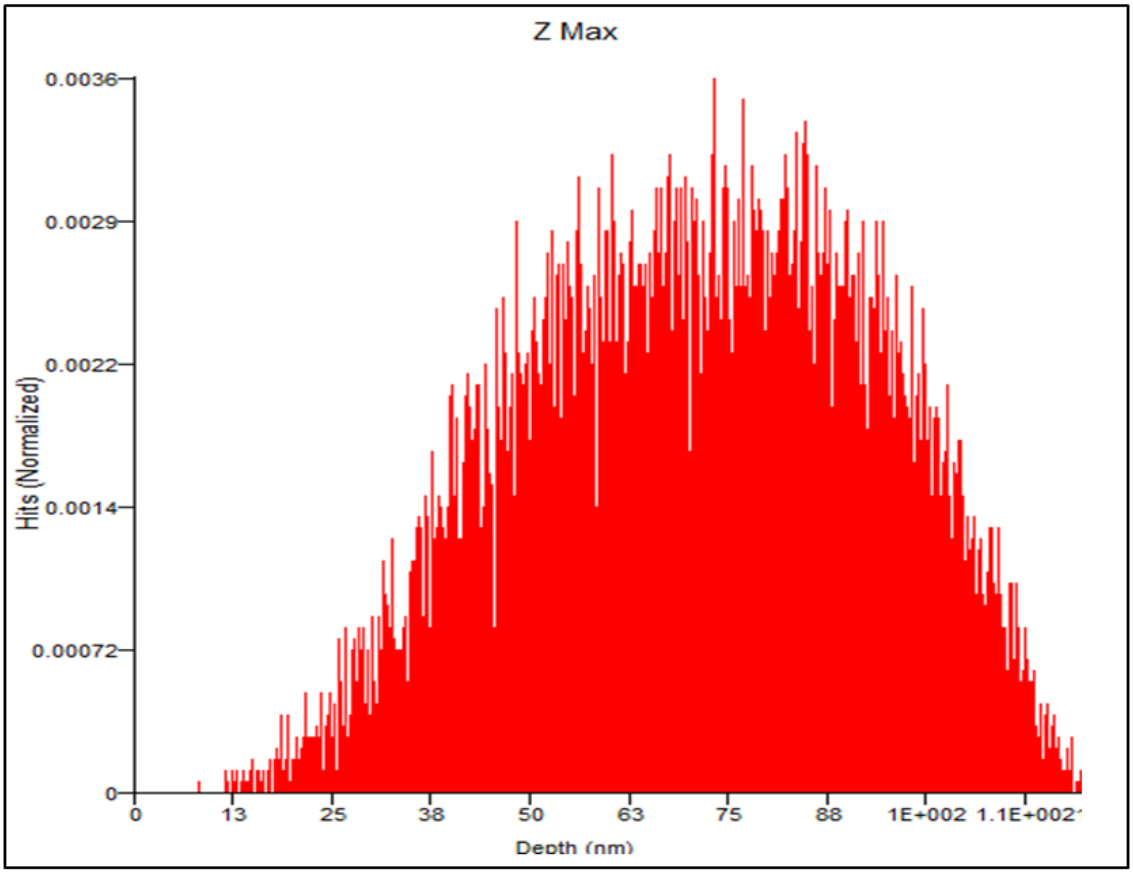

Figure A-1: Electron penetration depth for 2 keV electrons in LTB.

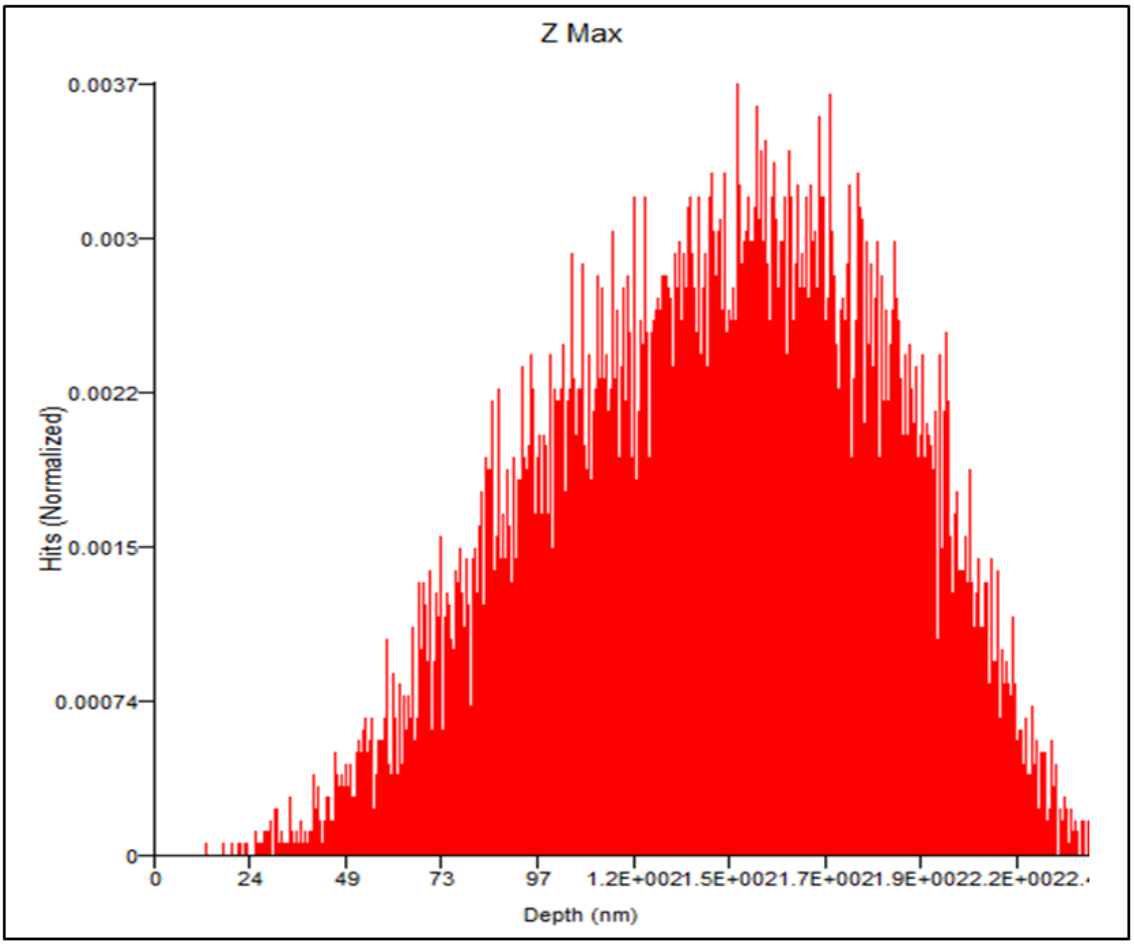

Figure A-2: Electron penetration depth for 3 keV electrons in LTB.

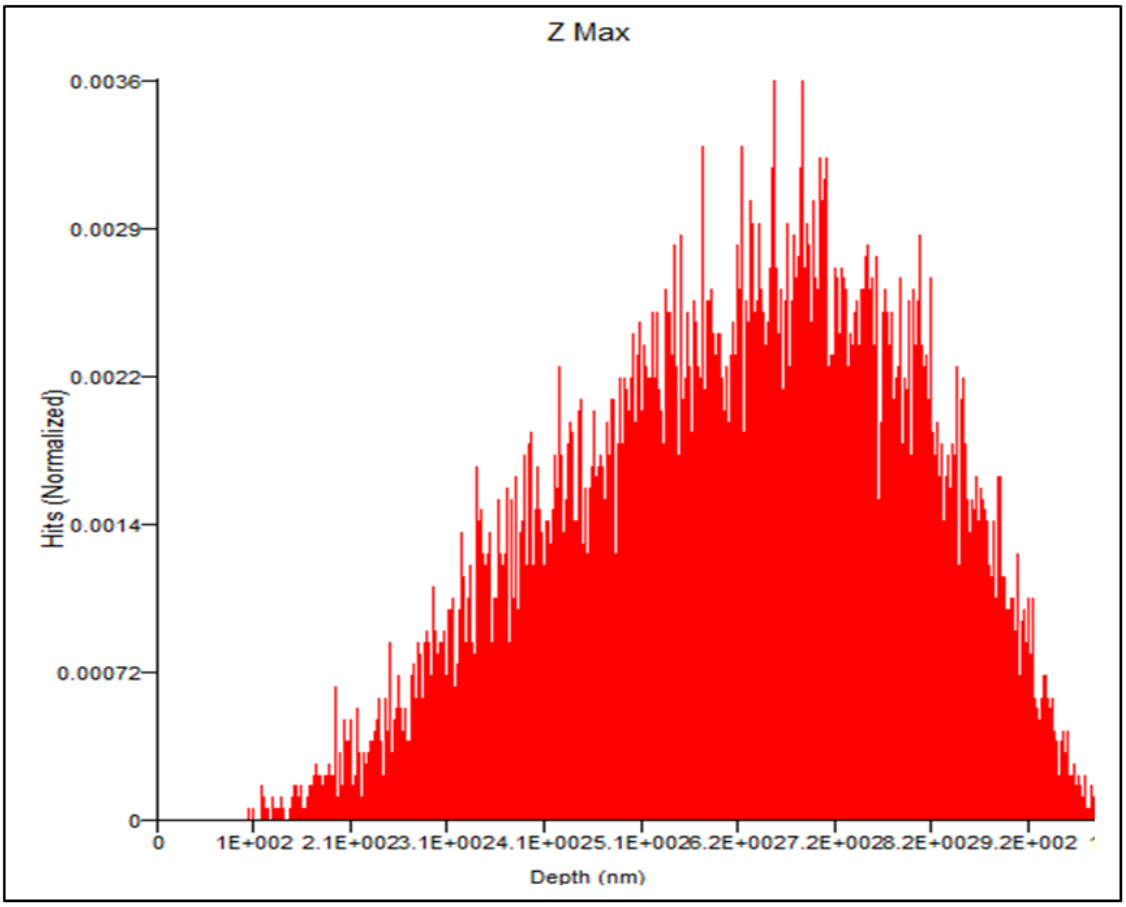

Figure A-3: Electron penetration depth for 7 keV electrons in LTB.

VIII. Appendix B: Electron Beam Current and Energy Studies

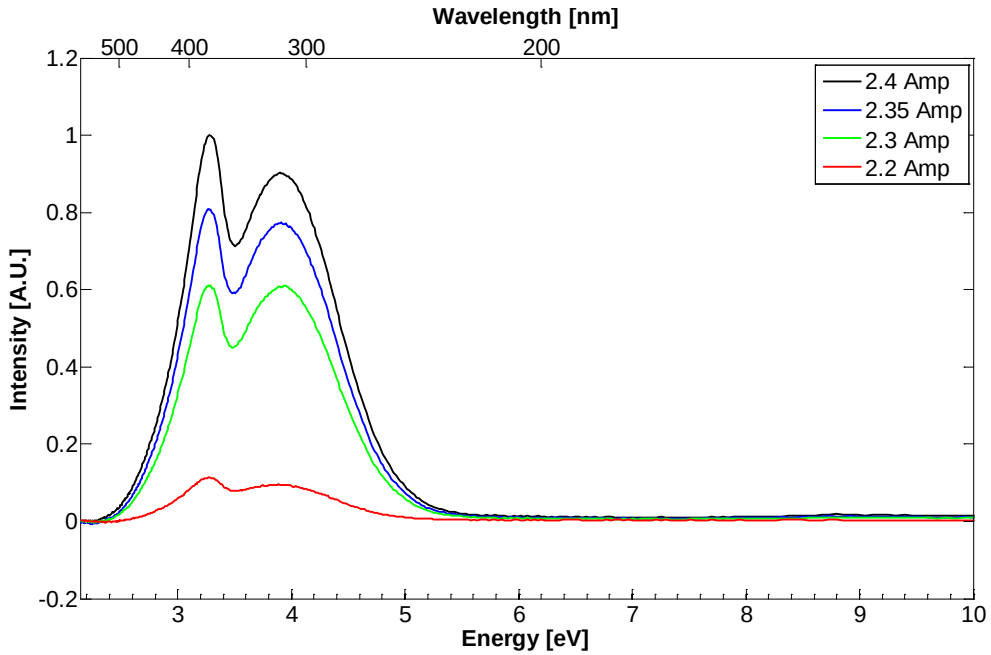

Figure B-1: This plot shows the results of a parametric study of the electron beam current conducted on the 2nd generation Ukrainian undoped sample at room temperature. Note that the peaks do not shift in energy/wavelength. The only change was in the intensity of the peaks. This shows that saturation does not occur when using a 2.4 Amp filament current.

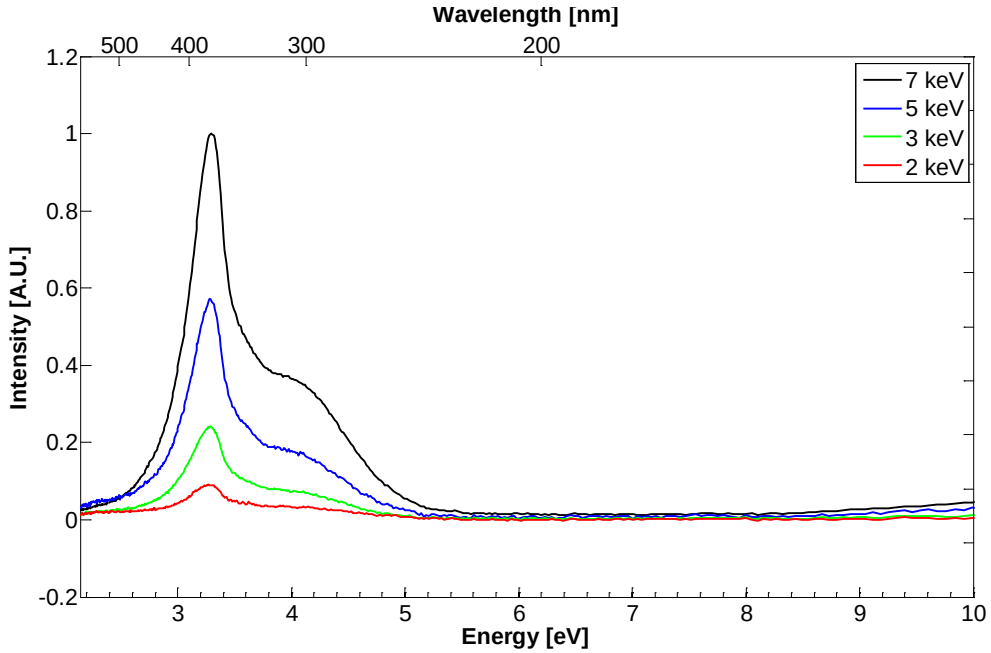

Figure B-2: This plot shows the results of a parametric study of the electron beam energy. Like beam current changes, beam energy variation does not change the nature of the results, only the intensity of their respective emissions. Therefore, using a 5 keV electron beam is adequate to analyze the bulk characteristics of the crystal.

9. Appendix C: NaCl and GaN Data

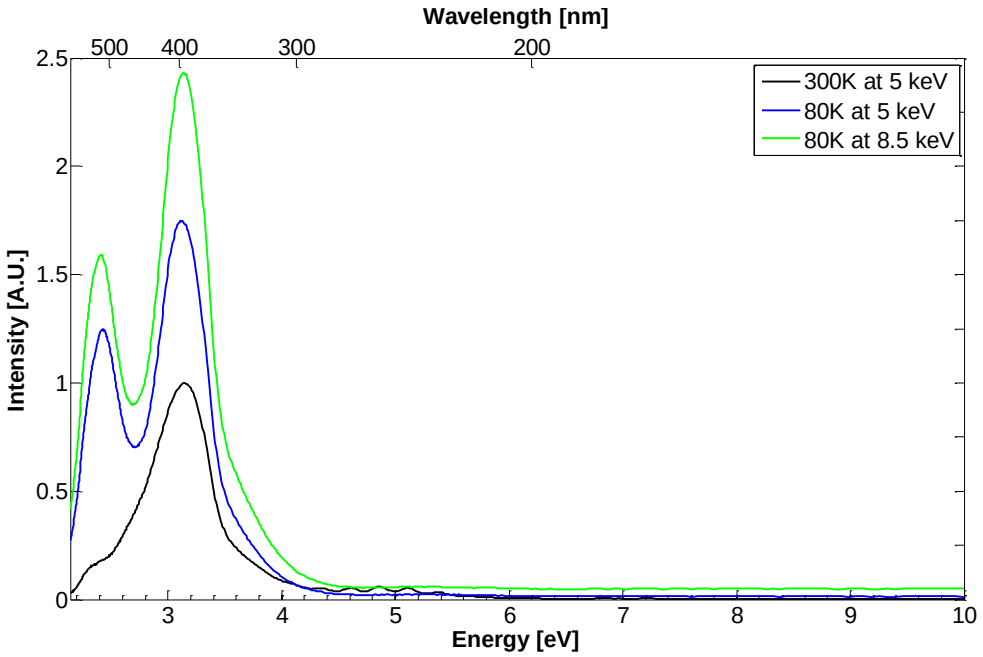

Figure C-1: Data taken from the VUV system on a NaCl single crystal. Peaks occur at 395 nm (3.14 eV) and 513 nm (2.42 EV). This is a fairly good match to previously measured luminescence occurring at 2.42 eV and 3.5 eV. [31]

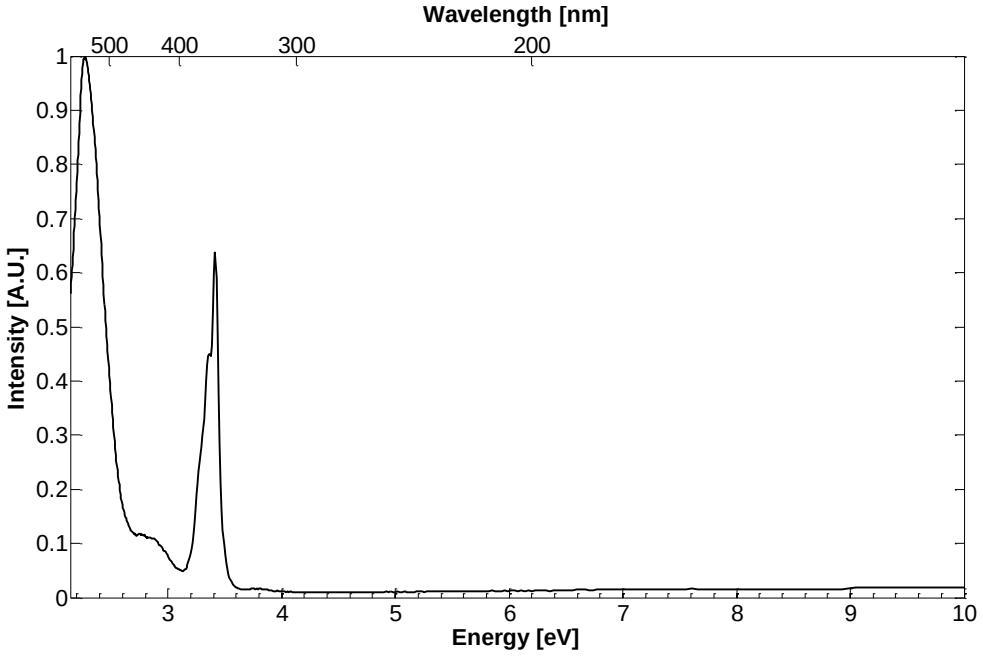

Figure C-2: Data taken on a crystalline GaN sample. A peak was observed at 363 nm (3.41 eV), which exactly matches the experimentally measured band gap of GaN at room temperature. [33]

REPORT DOCUMENTATION PAGE

Form Approved
OMB No. 074-0188

PLEASE DO NOT RETURN YOUR FORM TO THE ABOVE ADDRESS.

1. REPORT DATE *(DD-MM-YYYY)*	2. REPORT TYPE	3. DATES COVERED *(From – To)*
21-03-2013	Master's Thesis	August 2011 – March 2013

TITLE AND SUBTITLE

CATHODOLUMINESCENCE AND THERMOLUMINESCENCE OF UNDOPED LTB AND LTB:A (A = Cu, Ag, Mn)

5a. CONTRACT NUMBER

5b. GRANT NUMBER

5c. PROGRAM ELEMENT NUMBER

6. AUTHOR(S)

Hadfield, Zachary L., Major, USA

5d. PROJECT NUMBER

5e. TASK NUMBER

5f. WORK UNIT NUMBER

7. PERFORMING ORGANIZATION NAMES(S) AND ADDRESS(S)

Air Force Institute of Technology
Graduate School of Engineering and Management (AFIT/ENY)
2950 Hobson Way, Building 640
WPAFB OH 45433-8865

8. PERFORMING ORGANIZATION REPORT NUMBER

AFIT-ENP-13-M-13

9. SPONSORING/MONITORING AGENCY NAME(S) AND ADDRESS(ES)

Department of Homeland Security, Domestic Nuclear Detection Office
Samantha Kentis
245 Murray Lane SW
Washington, DC 20407
(202) 282-8000

10. SPONSOR/MONITOR'S ACRONYM(S)
DHS

11. SPONSOR/MONITOR'S REPORT NUMBER(S)

12. DISTRIBUTION/AVAILABILITY STATEMENT

APPROVED FOR PUBLIC RELEASE; DISTRIBUTION UNLIMITED.

13. SUPPLEMENTARY NOTES

14. ABSTRACT

The Department of Defense is interested in lithium tetraborate (Li2B4O7) crystals for their possible use as a solid state neutron detection material. With large concentrations of 6Li and 10B, it has a high neutron capture cross section. Furthermore, the crystal fluoresces in the presence of ionizing radiation, making it an attractive candidate for a scintillating detection device. However, there is a lack of fundamental knowledge about the material characteristics, particularly with regard to its fluorescent spectrum.

Cathodoluminescence measurements were conducted on undoped and doped samples of lithium tetraborate in order to characterize the nature of its fluorescent spectra under different environmental conditions. Measurements were made using a vacuum ultraviolet cathodoluminescence system specifically designed to detect high energy photons emitted in wide band gap materials. The cathodoluminescent spectra from 10 K to room temperature was characterized for six different lithium tetraborate crystals: three undoped crystals and one each doped with silver, copper, and manganese.

15. SUBJECT TERMS

Cathodoluminescence, Thermoluminescence, LTB, Lithium Tetraborate, $Li_2B_4O_7$

16. SECURITY CLASSIFICATION OF:			17. LIMITATION OF ABSTRACT	18. NUMBER OF PAGES	19a. NAME OF RESPONSIBLE PERSON
a. REPORT	b. ABSTRACT	c. THIS PAGE			Dr Hengehold, Robert ADVISOR
U	U	U	UU	92	19b. TELEPHONE NUMBER *(Include area code)* (937) 255-6565, ext 4502 (robert.hengehold@afit.edu)

Standard Form 298 (Rev. 8-98)
Prescribed by ANSI Std. Z39-18